Amman, October 29, 2006
(draft) Note: **M-04**

Design Study of an Elliptically Polarizing Undulator for SESAME

Hamed Tarawneh

1. INTRODUCTION

SESAME will be a third generation light source with electron energy of 2.5 GeV and 400 mA beam current. The SESAME users have defined their demands of the photon energy. One demand is an elliptically polarized light with an energy range of 100 eV to 1500 eV. In this note a proposed design of an elliptically polarizing undulator (EPU) is presented. The undulator has a period length λ_u of 60 mm, a magnetic gap of 13 mm and a total length of 1.782 m. The interaction of the EPU with the electron beam is presented. The feasibility to house the EPU in both long and short straight section has been investigated.

2. CHOICE OF THE EPU MAGNET PARAMETERS

The SESAME lattice [1] will define the minimum gap and the length of any insertion device (ID) in both the short and long straight sections in order to maintain a decent vacuum lifetime. The lifetime is an important issue for SESAME since the storage ring will be injected at 800 MeV beam energy.
The SESAME users demand a photon flux of 5×10^{14} photons/sec/0.1%BW [2] and low photon energy of less than 100 eV. To meet such demands, the proposed design of the EPU magnet has a magnetic gap of 13 mm, period length of 60 mm and 28 periods. This satisfies a stay clear aperture 8.5 mm for an ID length of about 2 m [1] and fundamental photon energy of elliptically polarized light less than 100 eV at minimum undulator gap.

3.1. MAGNETIC DESIGN AND LAYOUT

The Apple-II type helical undulator [3] has been chosen to achieve this demand. The magnet is a pure permanent magnet structure which composed of four sub-assemblies as shown in Figure 1. S1 and S3 are fixed, S2 and S4 are allowed to move longitudinally parallel to the magnetic axis (y-axis in the figure). The relative movement, called undulator phase, of the two sub-assemblies changes the strength of the magnetic field B_x and B_z and hence the polarization of the emitted radiation, i.e. horizontally, vertically and elliptically polarized source.
The design calculations have been done using RADIA code from ESRF [4] and using MATHEMATICA as a front end. The permanent magnetic material (PM) used in the calculations is NdFeB with B_r= 1.22 T with a relative permeability of 1.05 parallel to and 1.17 perpendicular to the easy axis of the blocks. The blocks have a thickness of ¼ period and 40 mm × 40mm cross section with 5 mm × 5mm cuts needed to clamp the blocks in the holders, see Figure 2. The main parameters of the SESAME EPU are summarized in Table 1.

Table 1. SESAME EPU main parameters.

Magnet period [mm]	60
Number of periods	28
Magnetic gap [mm]	13
Max. gap between adjacent assemblies [mm]	1
PM material	NdFeB with B_r=1.22T
Block dimension	15 mm × 40mm × 40mm
Cuts dimension	5 mm × 5 mm

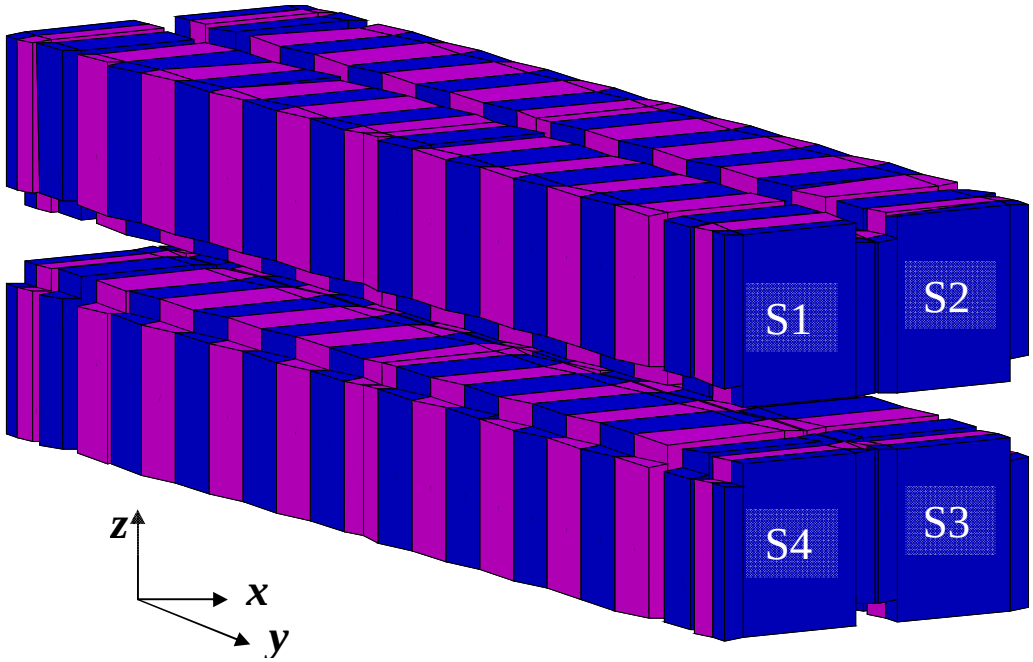

Figure 1. Four sub-assemblies schematic of SESAME EPU.

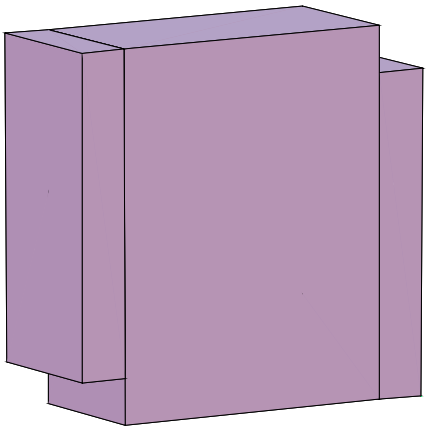

Figure 2. One permanent magnetic material block.

3.2. MODES OF OPERATIONS

Three modes of operation are foreseen for this magnet;

1. Horizontally polarized mode: an undulator phase of 0 mm.
2. Vertically polarized mode: an undulator phase of $\lambda_u/2$ mm.
3. Elliptically polarized mode: an undulator phase between 0 mm and $\lambda_u/2$ mm.

The inclined mode of operation has not been considered for this magnet. The inclined polarized light is achieved by moving the assemblies S2 and S4 longitudinally but opposing each other.

3.3. END BLOCKS CONFIGURATION

It is important that there is no net change in angle or transverse position on the electron beam in the EPU undulator, i.e. zero first and second field integrals [5, 6]. This effect, determined by the non-unit permeability of the PM material, can be significantly minimized by the design of the end blocks of the magnet [7, 8]. The Elettra scheme has been used for the SESAME EPU which makes use of half-thickness ($\lambda_u/8$) blocks with spaces (A1, A2, A3) that are numerically optimized to reduce the field integrals [8], see Figure 3. The length of the full-size magnet is 1.752 m and by adding half a period length for the longitudinal translation of the two sub-assemblies, a total length of 1.782 m needed to house this magnet.

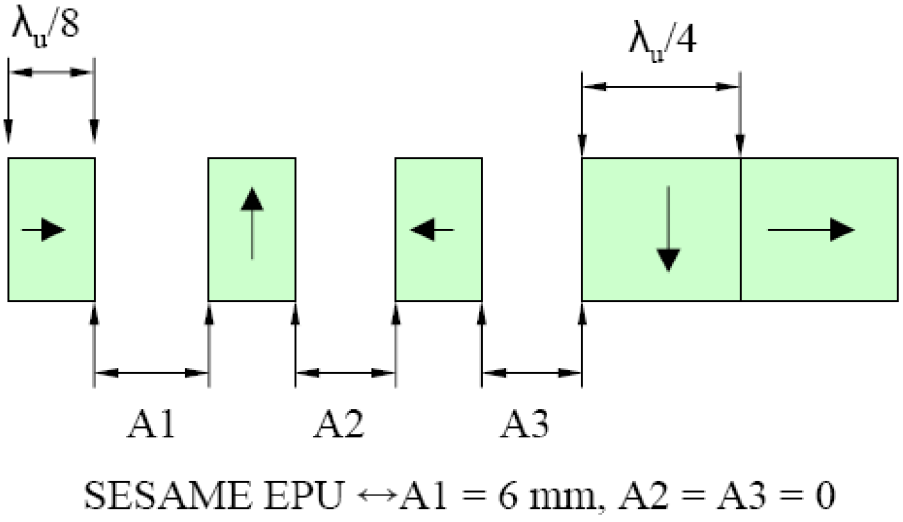

Figure 3. End blocks configuration for SESAME EPU.

The criteria specifications on the field integrals for the SESAME EPU are as below;

$$\text{First Integral:} \quad \int B_{x,z}(x = z = 0)dy \le 100 G.cm$$

$$\text{Second Integral:} \quad \iint B_{x,z}(x = z = 0)dy'dy \le 10^5 G.cm^2$$

3.4. FLUX DENSITIES AND FIELD INTEGRALS

An asymmetric layout has been adopted for the SESAME EPU, i.e. the vertical field has the same polarities at the entrance and exit of the magnet. The magnetic flux densities B_x (horizontal) and B_z (vertical) for an EPU device can be written as follows

$$B_z(0,0,s) = B_{z0}.\cos(\frac{\phi}{2}).\sin(\frac{2\pi}{\lambda_u}y + \frac{\phi}{2})$$

$$B_x(0,0,s) = -B_{x0}.\sin(\frac{\phi}{2}).\cos(\frac{2\pi}{\lambda_u}y + \frac{\phi}{2})$$

$$\phi = 2\pi\frac{\Delta y}{\lambda_u}$$

Where ϕ is the undulator phase and Δy is the longitudinal translation of the assemblies in meter.

The magnetic flux density on-axis for the three modes of operations as a function of undulator gap and phase are shown in Figures 4. The fundamental photon energies are shown in Figure 5. Table 2 summarizes the main magnetic properties of the SESAME EPU at minimum gap.

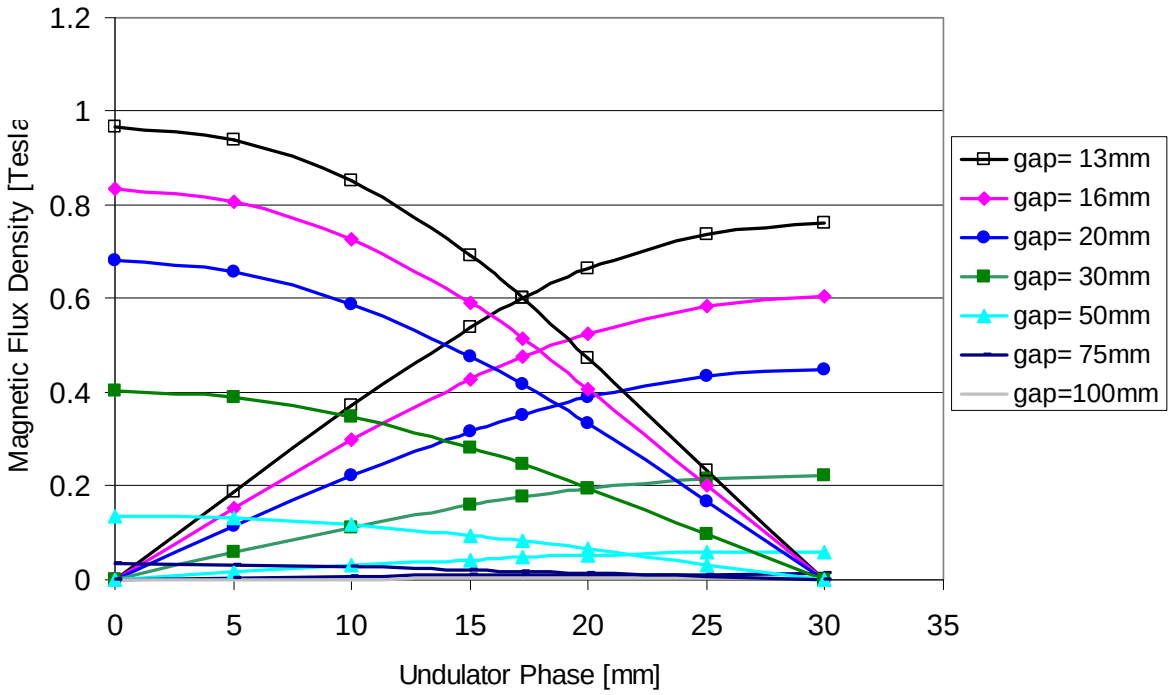

Figure 4. On-axis magnetic flux densities of the SESAME EPU.

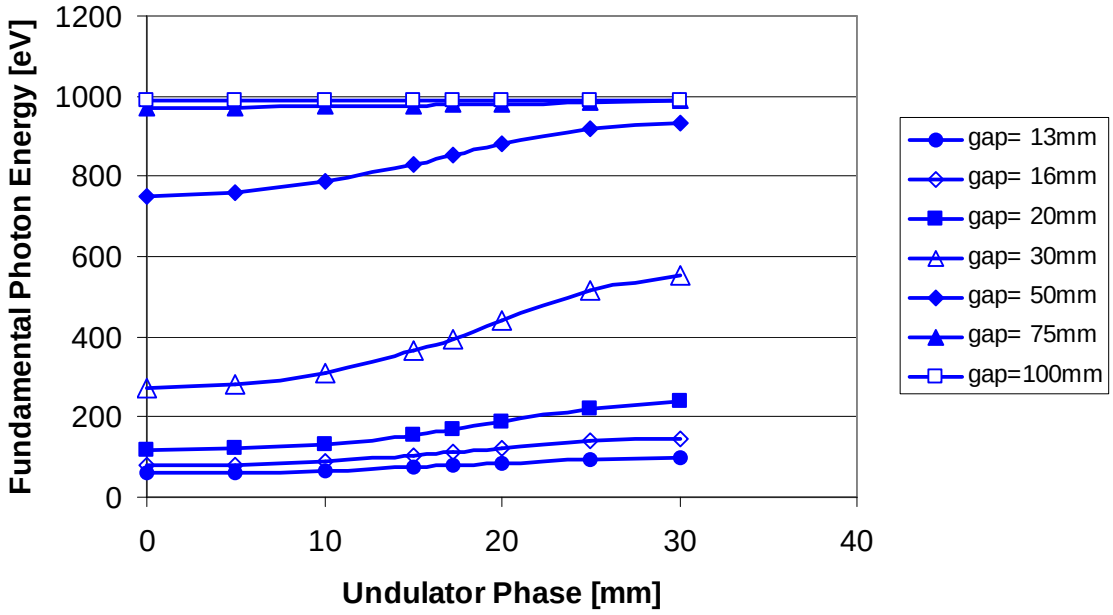

Figure 5. Fundamental photon energies of the SESAME EPU.

Table 2. Flux densities, k-values and minimum photon energies at minimum gap of 13mm.

Undulator Phase	Horizontal Flux Density (T)	Vertical Flux Density (T)	k-value	Photon Energy (eV)
Horizontal 0 mm	-	0.9724	5.44	62
Circular 17.2 mm	0.60	0.60	3.36	79
Vertical 30 mm	0.7617	-	4.26	98

The magnetic flux densities, both longitudinal and transverse, for a 10-periods model at minimum gap of 13 mm for the three modes of operation are shown in Figures 6 to 11. The dip at x=0 in Figure 7 is due to the 1 mm separation distance between the left and the right assemblies of the magnet. This effect, called transverse roll off, will result in different flux densities seen by the electron far out from the centre of the transverse phase space. This focusing effect leads to an angular kick of the off-centre electron and, hence, reduces the dynamic aperture of the storage ring, see Section 4.3. The transverse roll off becomes very strong for the vertical mode of operation as shown in Figure 11.

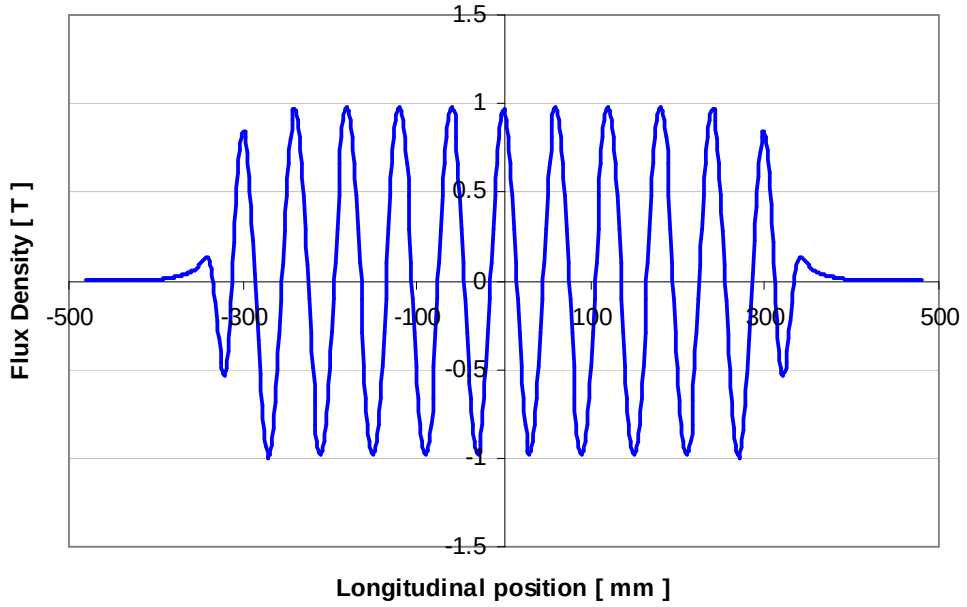

Figure 6. Longitudinal flux density for the horizontal undulator phase at minimum gap.

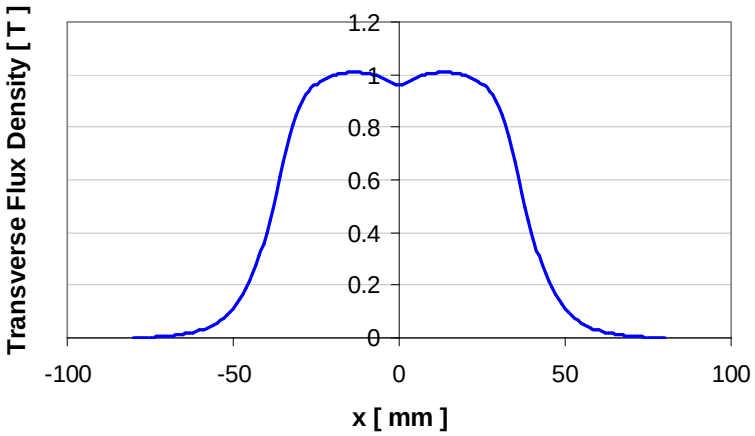

Figure 7. Transverse flux density of the horizontal undulator phase at minimum gap.

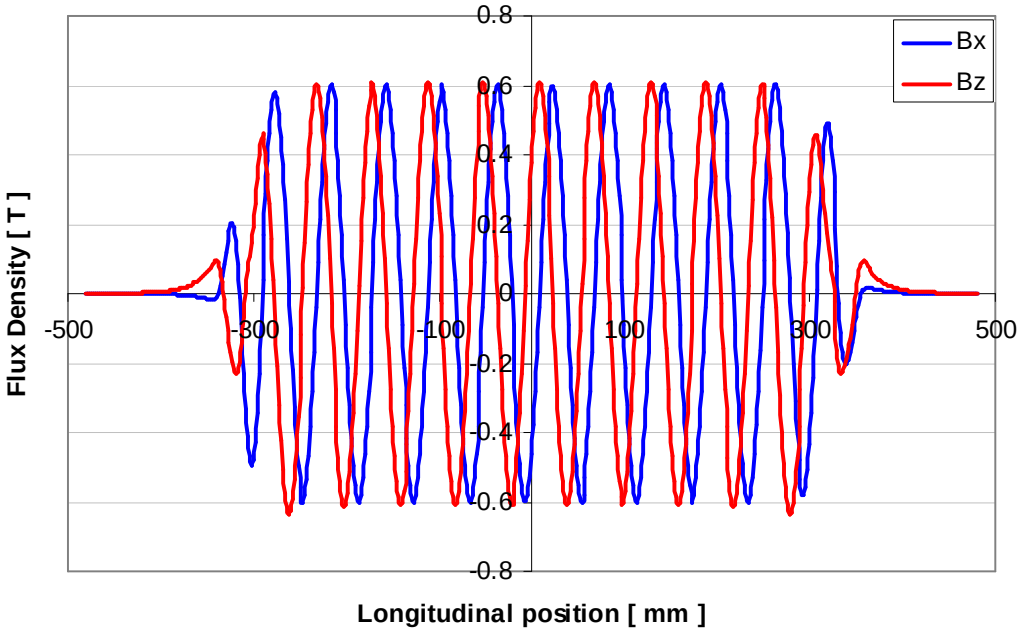

Figure 8. Longitudinal flux density for the circular undulator phase at minimum gap.

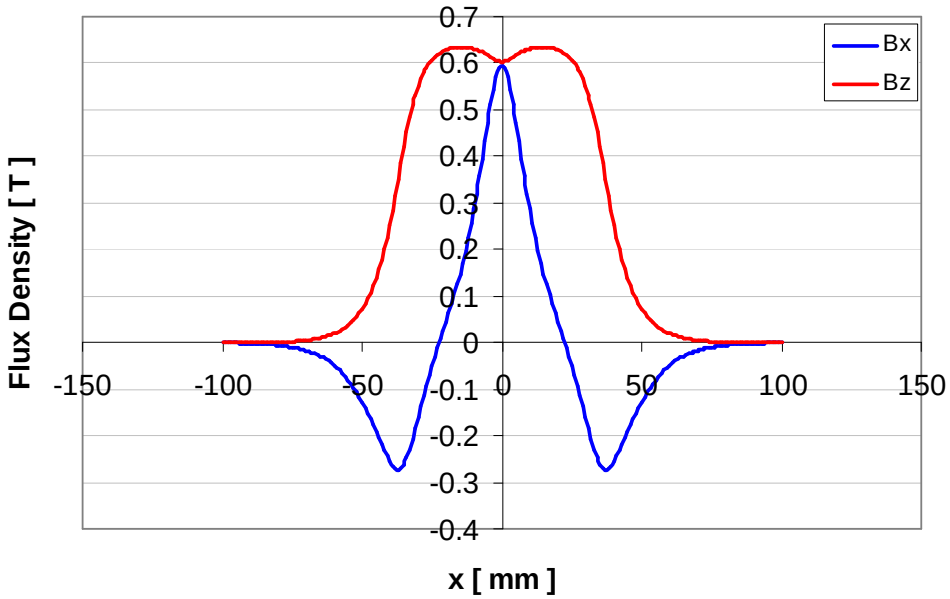

Figure 9. Transverse flux density of the circular undulator phase at minimum gap.

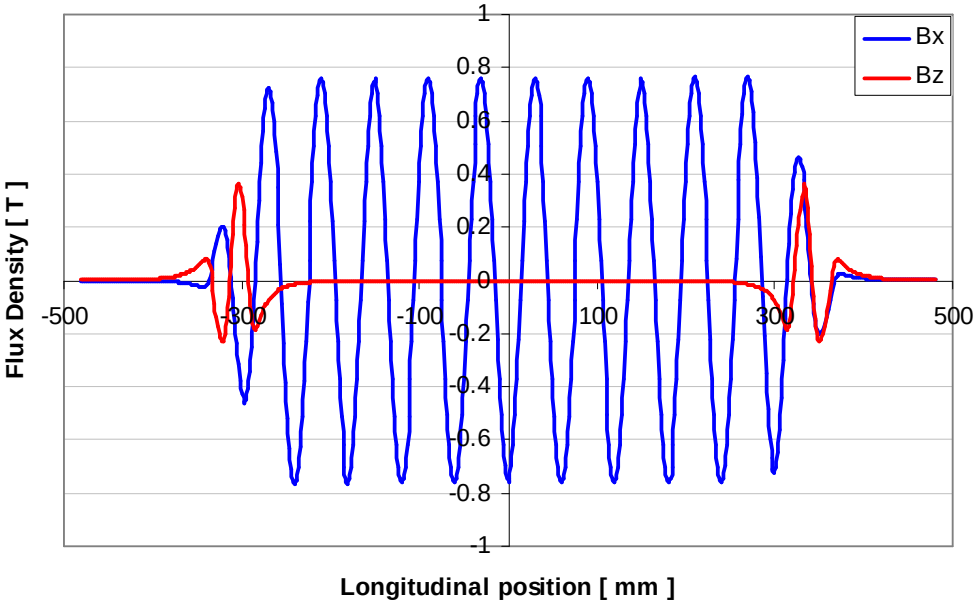

Figure 10. Longitudinal flux density for the vertical undulator phase at minimum gap.

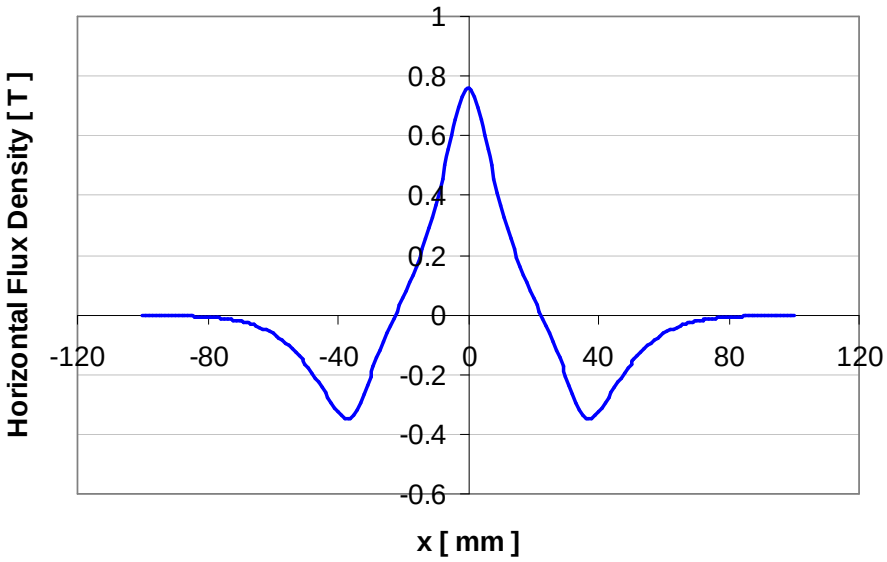

Figure 11. Transverse flux density of the vertical undulator phase at minimum gap.

As mentioned in Section 3.3, the end block configuration is capable of reducing the first and second field integrals below the specified limits without using passive (shimming technique) or active (trim coils) correction schemes at this stage of the design. Figure 12 shows the on-axis first field integral at minimum gap as a function of the undulator phase. The values are still less than 20% of the specified limit. Figure 13 shows the first field integral for the three modes of operation at minimum gap as a function of the transverse x-axis. The values for x = ±25mm are within 35% of the specified limit.

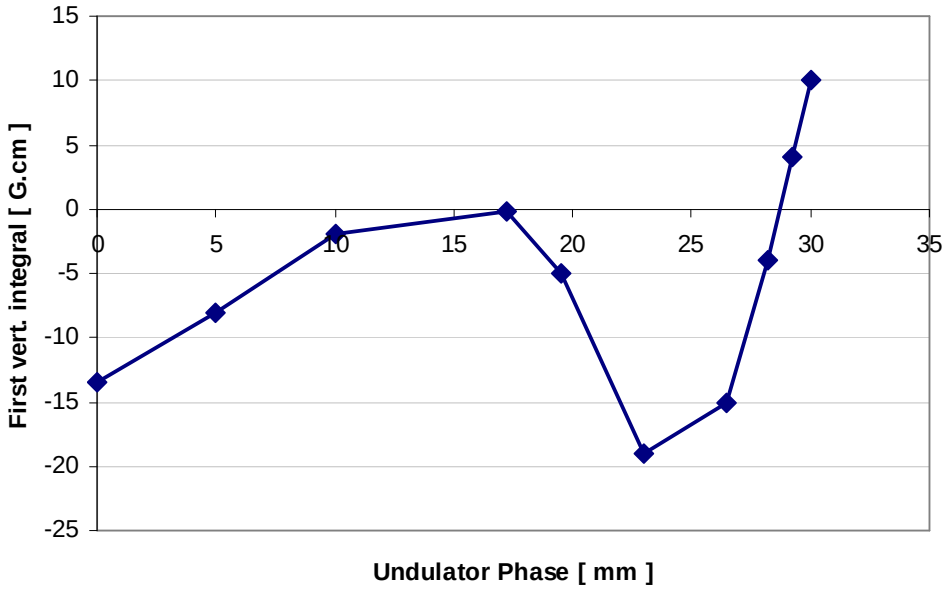

Figure 12. On-axis first field integral of the SESAME EPU at minimum gap.

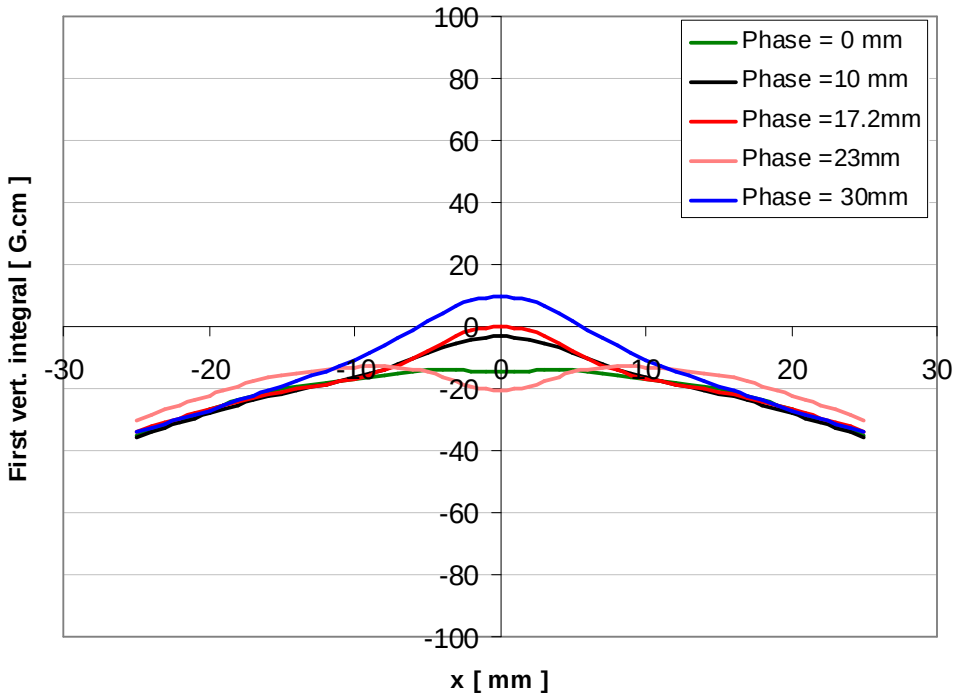

Figure 13. First field integral as function of x-axis at minimum gap.

Figures 14 to 19 show the electron beam orbit, both longitudinal and projected on the xz-plane, through the 10-periods model magnet. We could see that the maximum orbit offset inside the EPU is about 24 μm horizontally for the planar mode and -3 μm vertically for the vertical mode. The second integral of the full size magnet can be extrapolated from the model. The results for the second field integrals and the beam position at the magnet exit are shown in Table 3. All values of the second integrals are within the specified limits, expect for the case of B_z for the planar mode of operation. This can be easily reduced by using a long correction (trim) coils with vertical field.

Table 3. The second integrals and beam position at the exit of the SESAME EPU.

Phase	$\iint B_x.dy'dy$ [G.cm^2]	Beam Position [μm]	$\iint B_z.dy'dy$ [G.cm^2]	Beam Position [μm]
Horizontal	0	0	10640	12.72
Circular	520	0.62	7280	8.74
Vertical	2996	3.60	5392	6.47

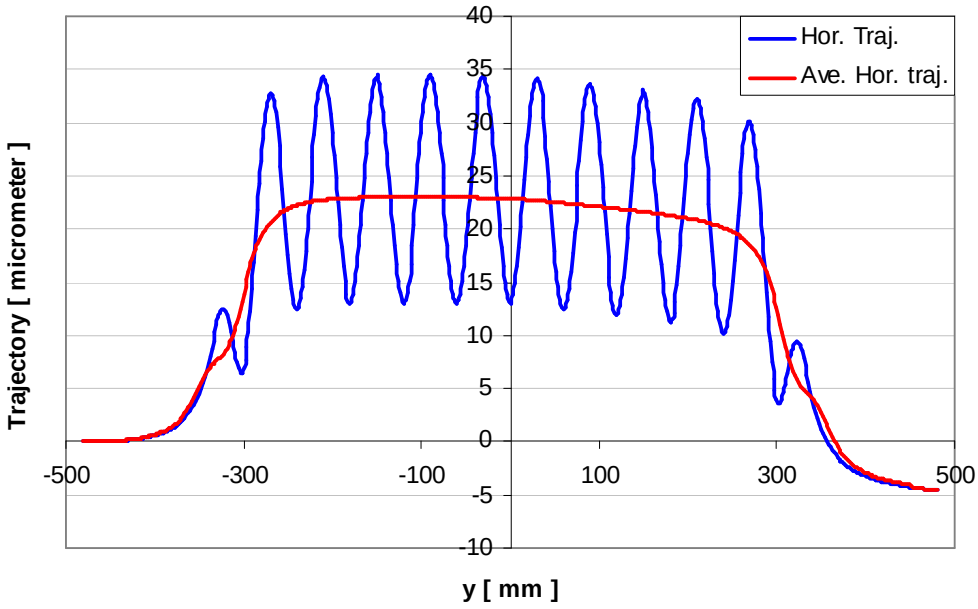

Figure 14. The 2.5 GeV electron trajectory in the model magnet for the horizontal undulator phase.

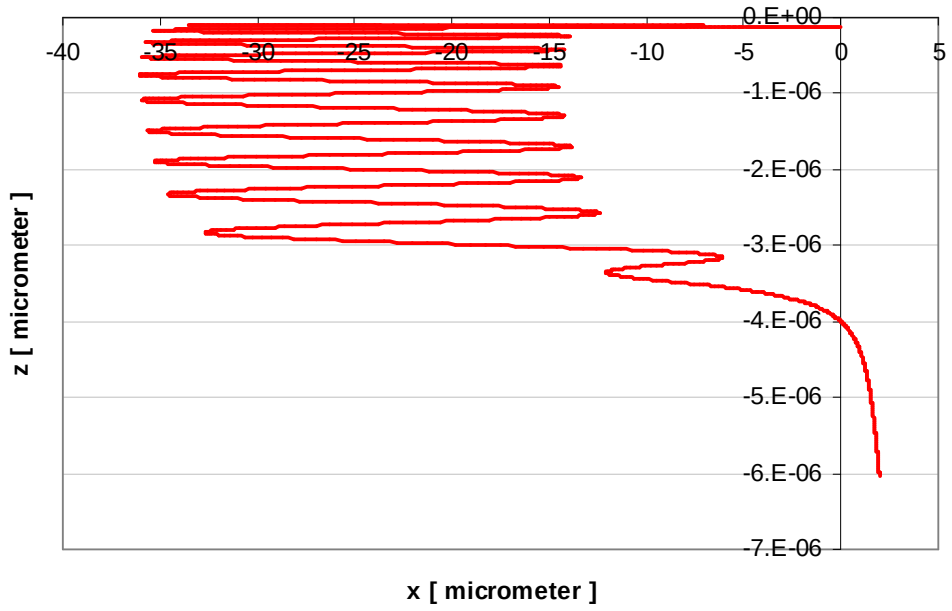

Figure 15. The 2.5 GeV electron trajectory in the xz-plane for the horizontal undulator phase.

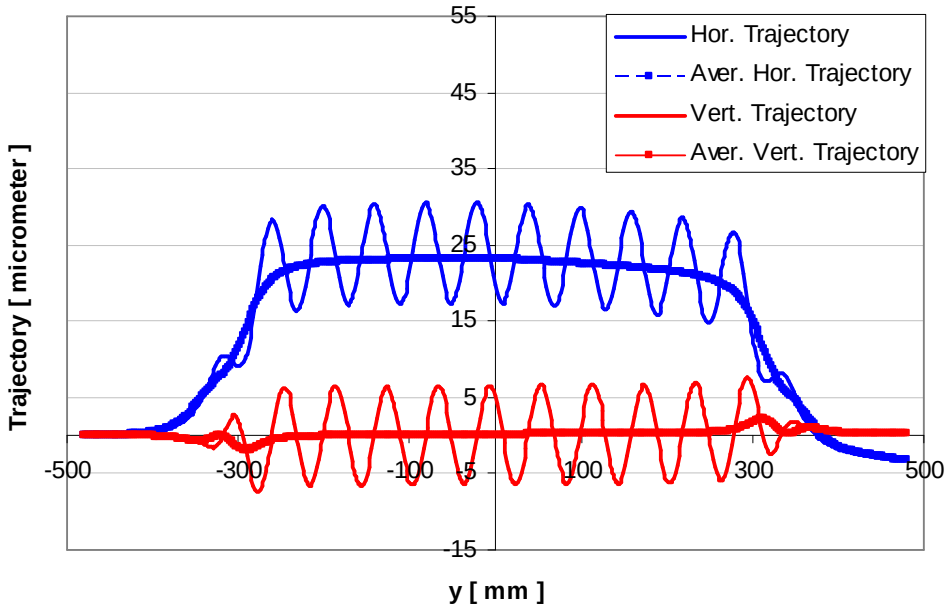

Figure 16. The 2.5 GeV electron trajectory in the model magnet for the circular undulator phase.

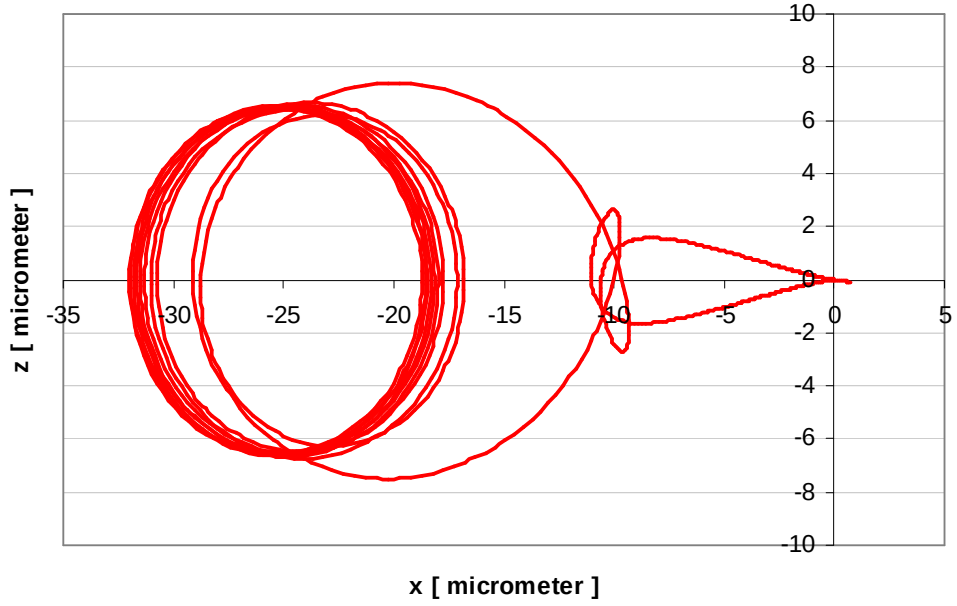

Figure 17. The 2.5 GeV electron trajectory in the xz-plane for the circular undulator phase.

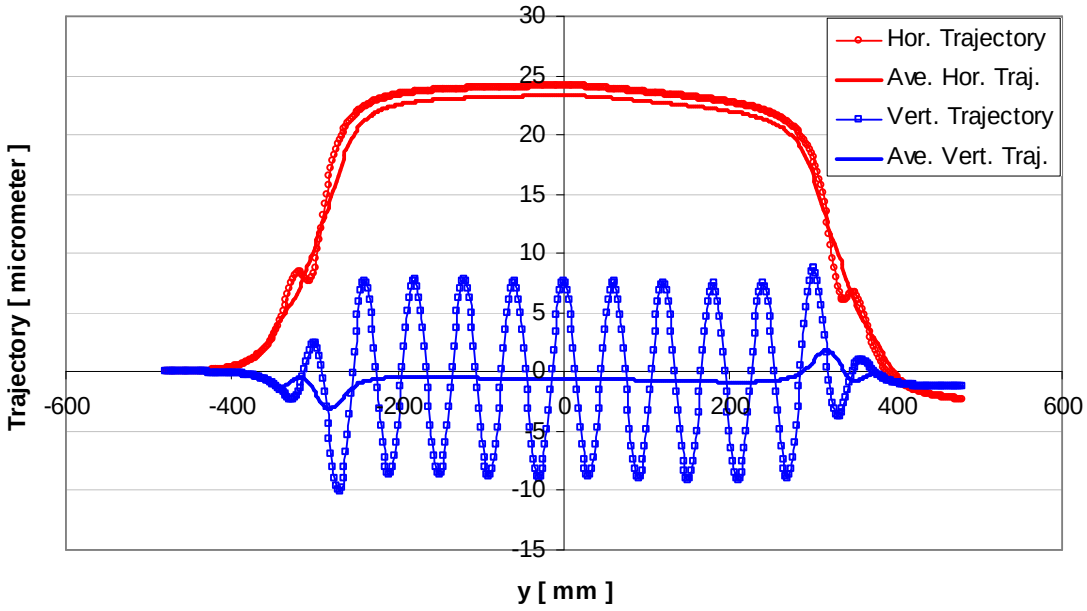

Figure 18. The 2.5 GeV electron trajectory in the model magnet for the vertical undulator phase.

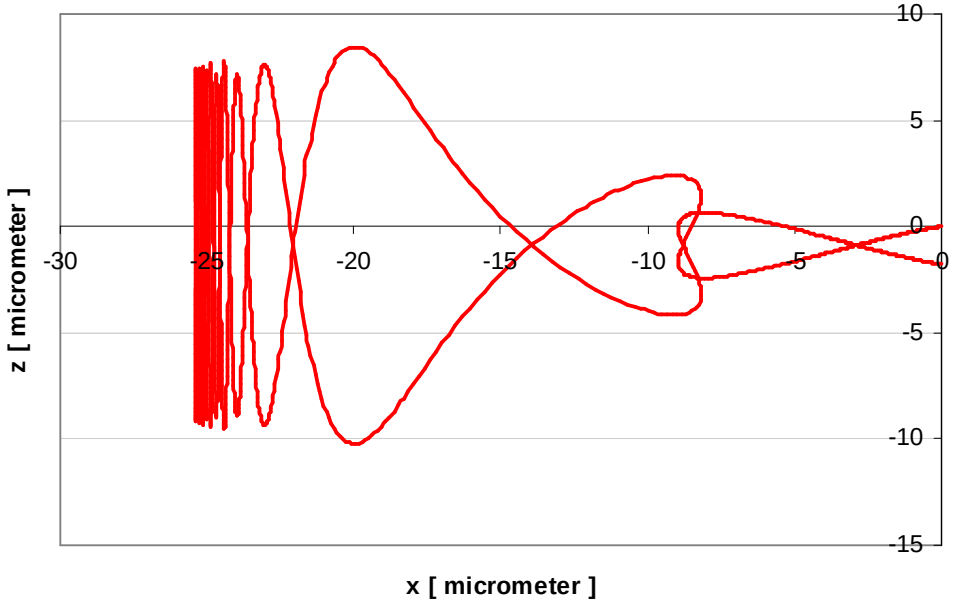

Figure 19. The 2.5 GeV electron trajectory in the xz-plane for the vertical undulator phase.

4. INTERACTION BETWEEN EPU AND ELECTRON BEAM

4.1. FOCUSING POTENTAIL

The transverse roll off of the magnetic flux results in an angular kicks and, hence a tune shift. This is expressed by a focusing potential given by [7, 9];

$$\Phi(x,z) = -\frac{1}{2}\left(\frac{e}{\gamma mc}\right)^2 \int_{-\infty}^{\infty}\left(\left(\int_{-\infty}^{z} B_x(x,z,y')dy'\right)^2 + \left(\int_{-\infty}^{z} B_z(x,z,y')dy'\right)^2\right)dy$$

where e is the electron charge, γmc the electron momentum and B_x and B_z the horizontal and vertical components of the magnetic flux density. The integrals can be solved analytically if we keep only the dominant n = 1 Fourier component of the flux density.

$$\Phi(x,z) = -\frac{L}{2}\left(\frac{ec\lambda_u}{2\pi E_e}\right)^2 \left(B_{1,x}(x,z)^2 + B_{1,y}(x,z)^2\right) = \frac{\Psi(x,z)}{E_e^2}$$

where L is the length of the undulator, λ_u the undulator period length, E_e the electron beam energy and $B_{1,x}$ and $B_{1,z}$ the n = 1 component in the Fourier expansion. This is a very good approximation for PPM undulators, where the n = 1 component dominates. The potential is largest at minimum gap, where the flux density is largest, and decreases rapidly with increasing gap.
The energy-independent part of the potential Ψ(x,z) at minimum gap is shown in Figures 20 – 22 for the Horizontal, Circular and Vertical modes of operation.

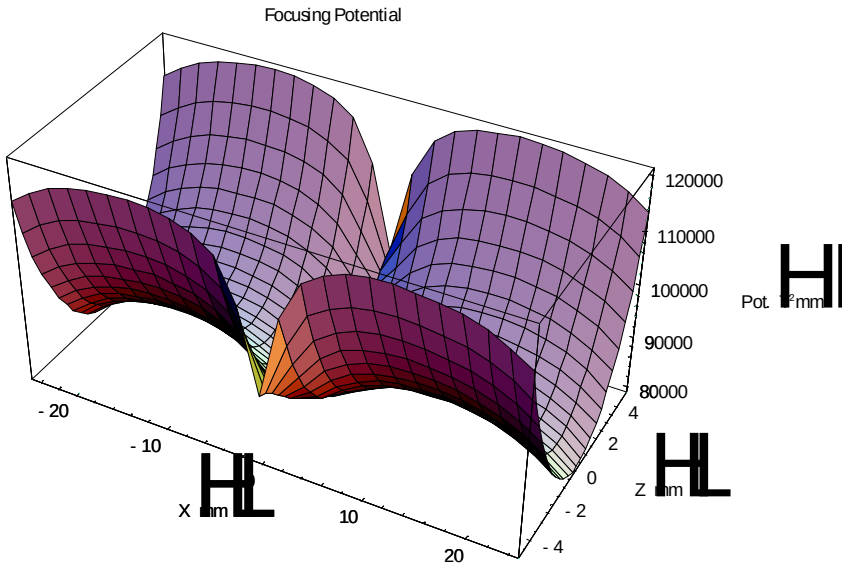

Figure 20. The focusing potential for the horizontal undulator phase at minimum gap

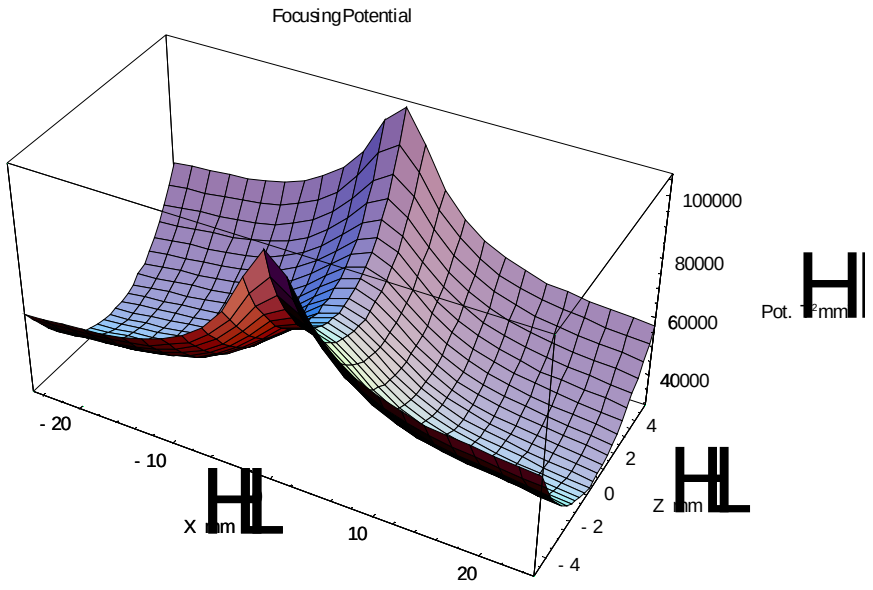

Figure 21. The focusing potential for the circular undulator phase at minimum gap

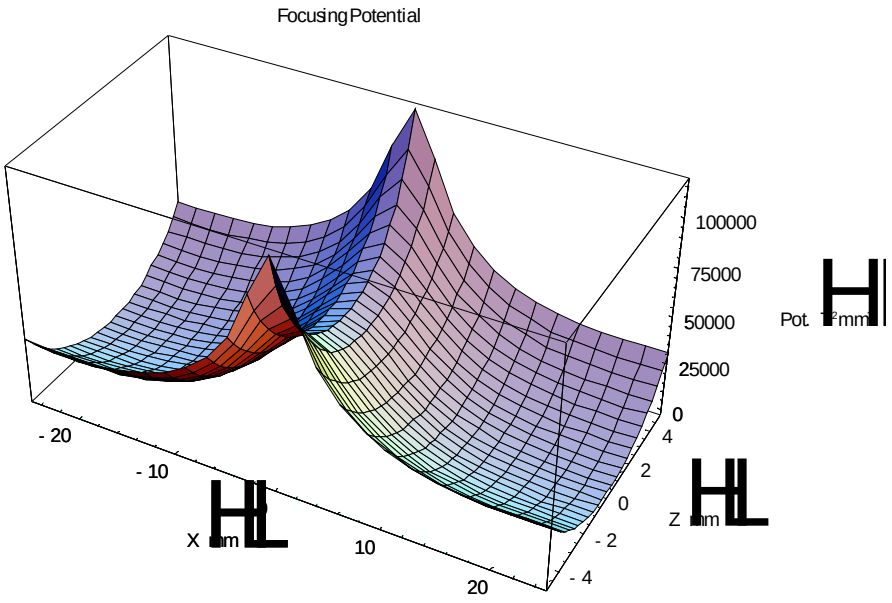

Figure 22. The focusing potential for the vertical undulator phase at minimum gap

4.2. ANGULAR KICK AND TUNE SHIFT

The horizontal θ_x and the vertical θ_z angular kicks the electrons will experience when traversing the undulator due to the transverse roll off are given by [7].

$$\theta_x = -\frac{\partial \Phi}{\partial x}$$

$$\theta_z = -\frac{\partial \Phi}{\partial z}$$

Figures 23 to 26 show the angular kick due to transverse roll off. In the vicinity of x=z=0, the kicks behave as being generated by an integrated quadrupole.

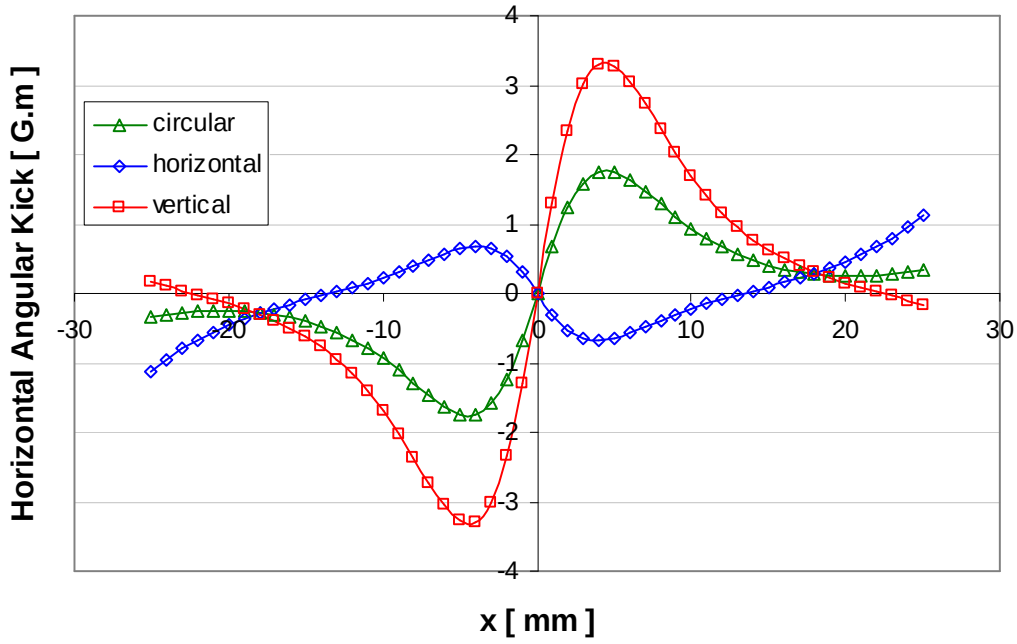

Figure 23. The horizontal angular kicks along the x-axis for all undulator phases at min. gap

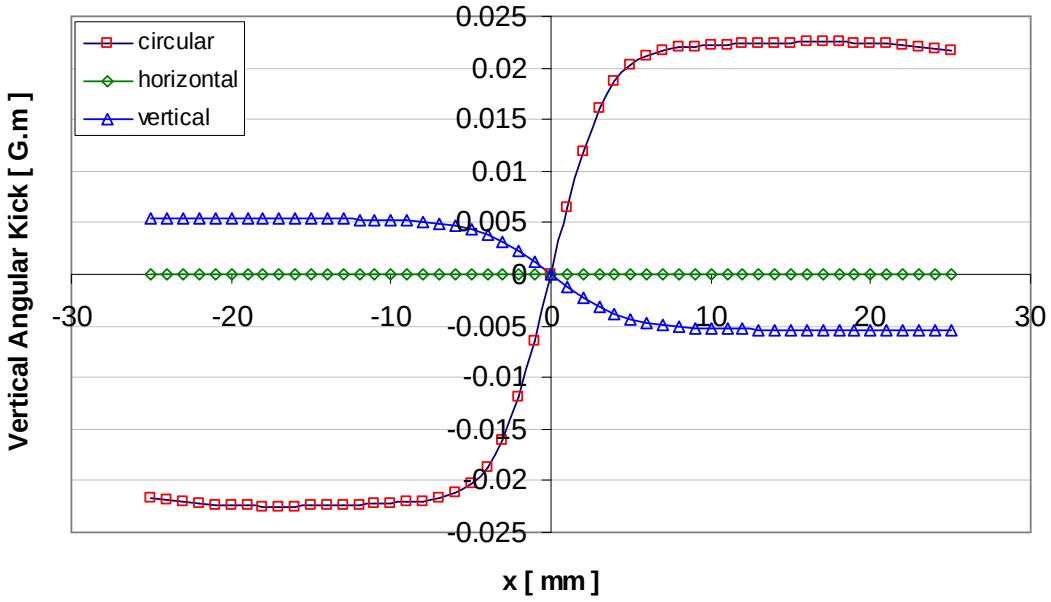

Figure 24. The vertical angular kicks along the x-axis for all undulator phases at min. gap

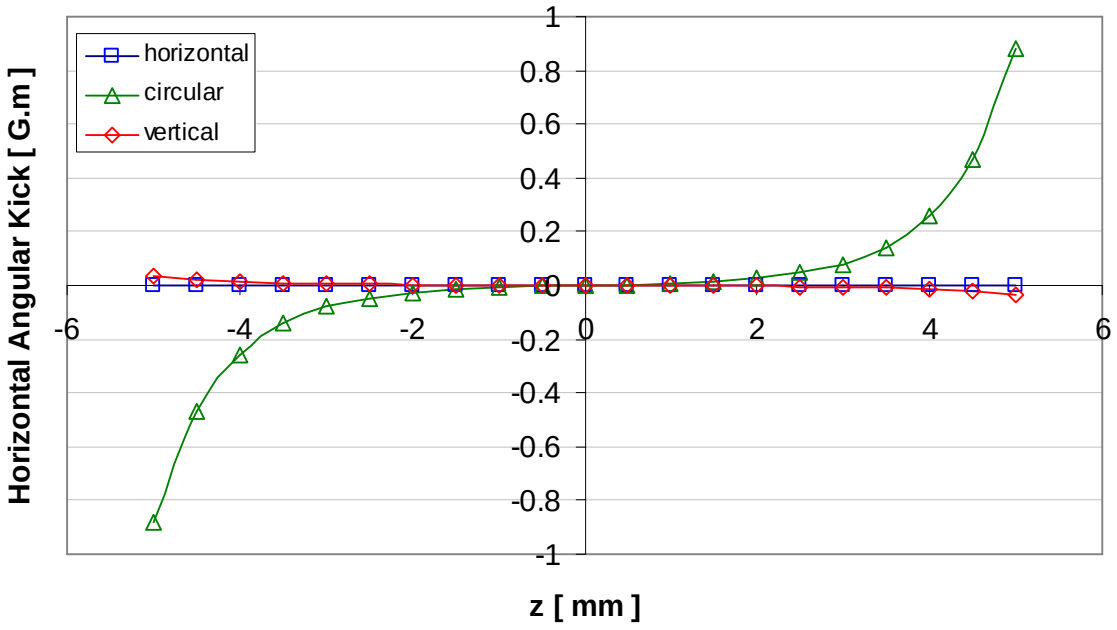

Figure 25. The horizontal angular kicks along the z-axis for all undulator phases at min. gap

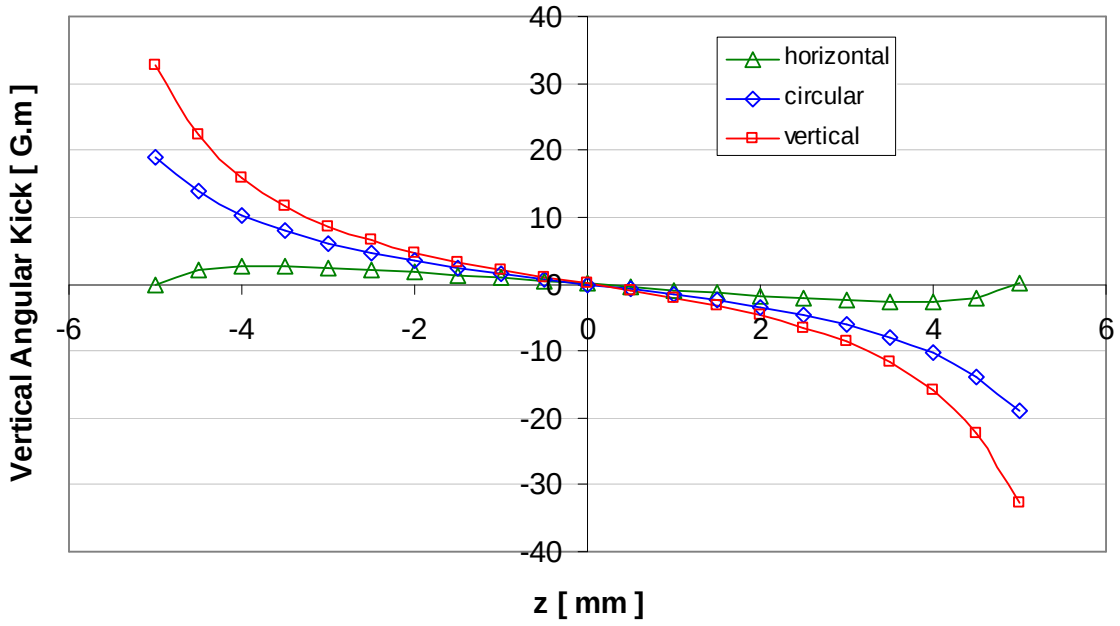

Figure 26. The vertical angular kicks along the z-axis for all undulator phases at min. gap

Depending on the position x,z of the electrons, focusing takes place due to the angular kicks. The focal lengths are given by [7];

$$\frac{1}{F_x} = -\frac{1}{2}\left(\frac{e}{\gamma mc}\right)^2 \int_{-\infty}^{\infty} \frac{\partial^2}{\partial x^2}\Phi(x,z,y)dy$$

$$\frac{1}{F_z} = -\frac{1}{2}\left(\frac{e}{\gamma mc}\right)^2 \int_{-\infty}^{\infty} \frac{\partial^2}{\partial z^2}\Phi(x,z,y)dy$$

Which induces a tune shift $\delta Q_{x,z}$ given by [10];

$$\delta Q_{x,z} = \frac{1}{4\pi}\frac{\beta_{x,z}}{F_{x,z}}$$

Where $\beta_{x,z}$ is the beta function at the location of the EPU magnet. The machine parameters used to evaluate the tune shifts are given in Table 4 at the middle of a short straight section of the SESAME lattice [1].

Table 4. Main parameters of the SESAME lattice.

Beam Energy	2.5 GeV
Beam Current	400 mA
Horizontal Emittance	25.7 nm.rad
Natural Energy Spread	1.086×10^{-3}
Coupling	1 %
Betatron function in the middle of short straight section	
$\beta_x / \alpha_x / \eta_x / \eta'_x$	13.30m / 0 / 0.53m / 0
$B_z / \alpha_z / \eta_z / \eta'_z$	0.77m / 0 / 0 / 0

Figures 27 to 30 show the horizontal and vertical betatron tune shifts on both x and z-axis's. The horizontal tune shift on the z-axis is a bit large mainly due to the large β_x at the EPU location. A possible cure for that is by running an electric current in a copper strips between the right and left sub-assemblies to generate a normal quadrupole component to locally compensate for the angular kick at different modes of operation.

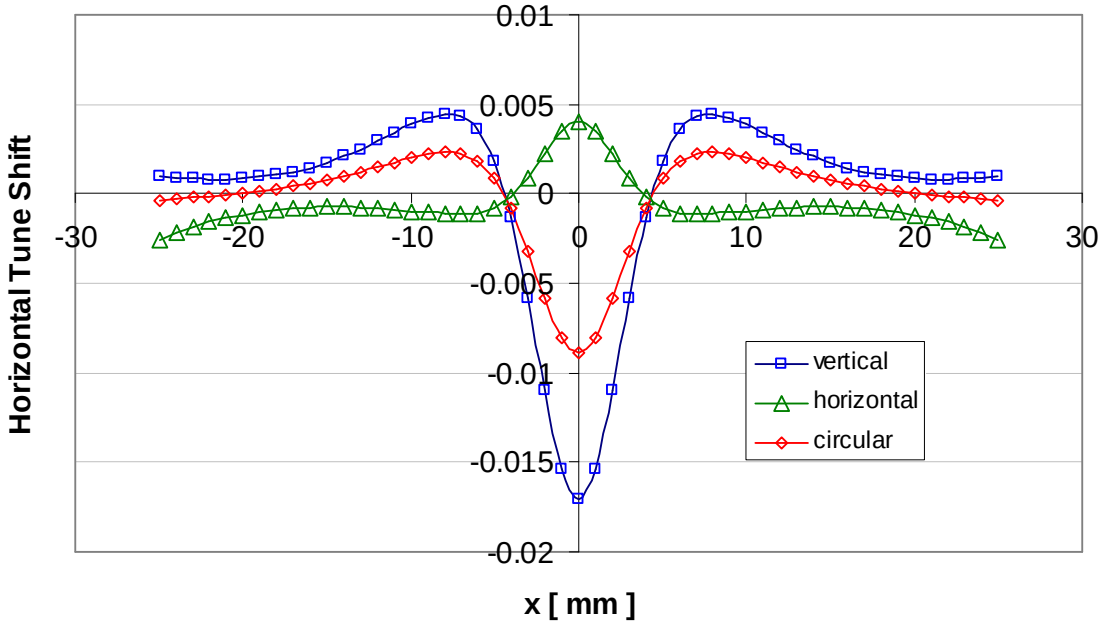

Figure 27. Horizontal tune shift across the x-axis for all undulator phases at min. gap.

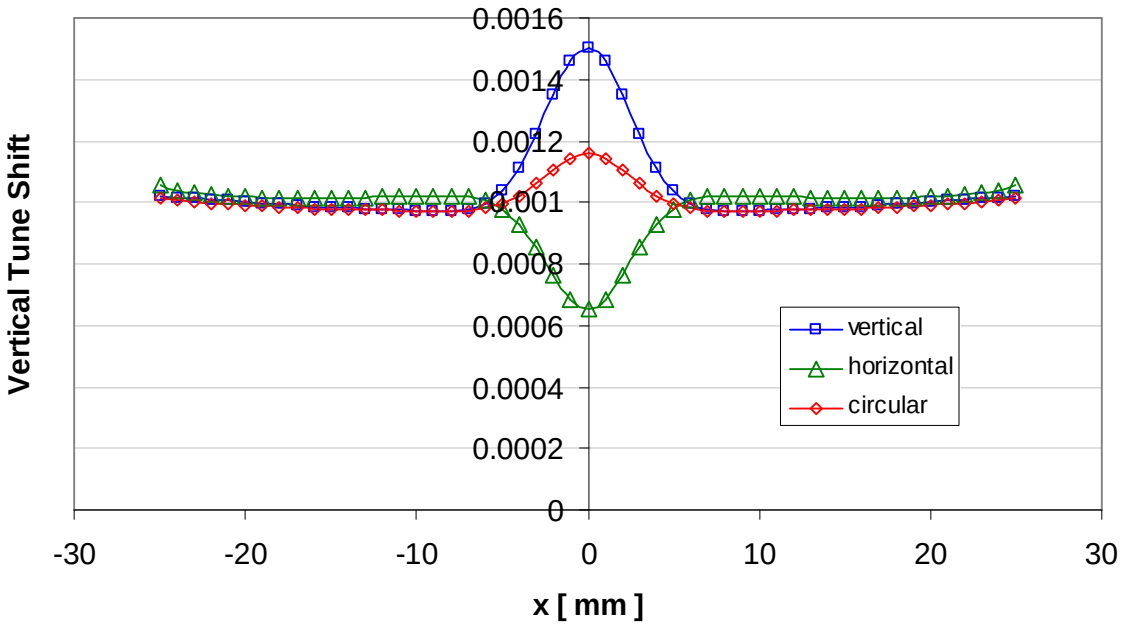

Figure 28. Vertical tune shift across the x-axis for all undulator phases at min. gap.

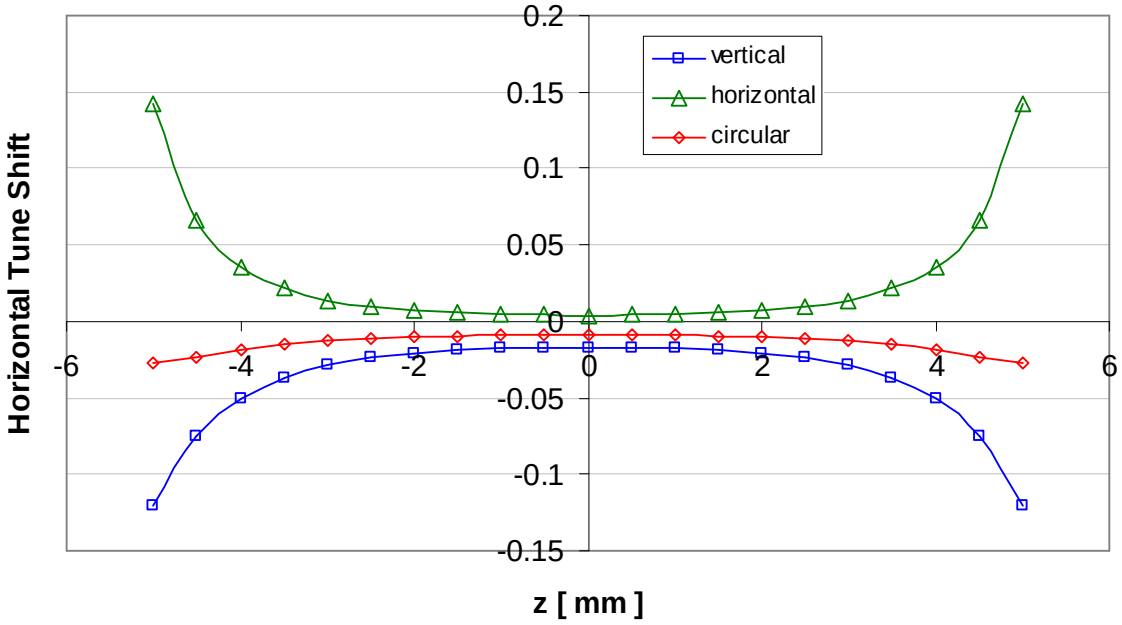

Figure 29. Horizontal tune shift across the z-axis for all undulator phases at min. gap.

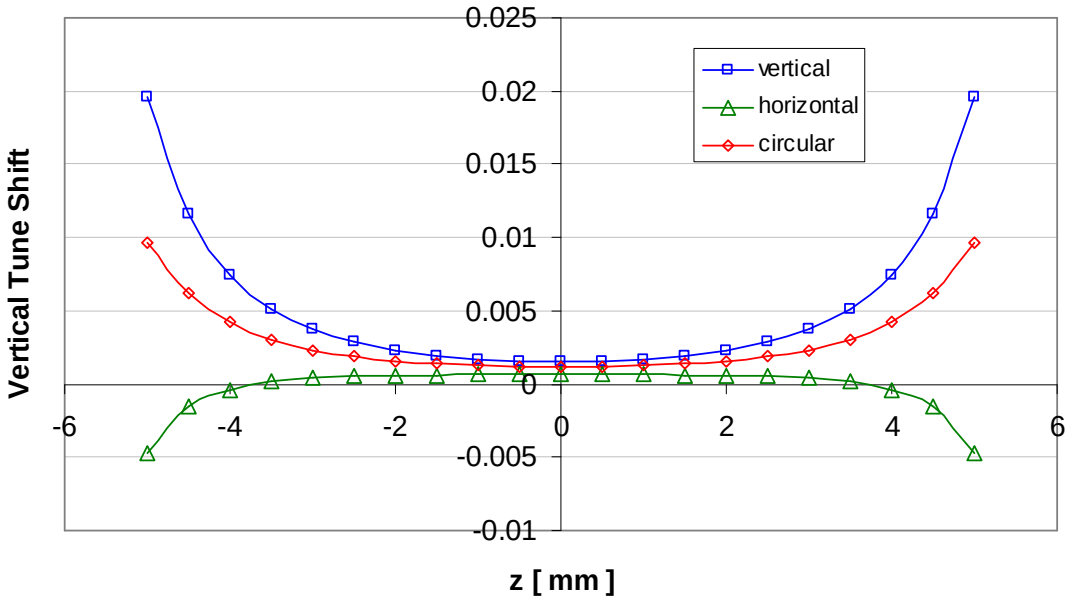

Figure 30. Vertical tune shift across the z-axis for all undulator phases at min. gap.

4.3. MACHINE FUNCTIONS AND DYNAMIC APERTURE

Installing an EPU device in the SESAME lattice will create a beta beat (associated with the tune shifts) in both planes since there are magnetic fields in both directions. In the BETA code any insertion device can be described by interpolation tables which provide an angular kick in T^2m^2 as a function of the coordinates of the particle passing that element, i.e. mapped insertion device [11].

Figures 31 to 33 show the effect of inserting an EPU device (mapped EPU) in a short straight section in the SESAME lattice, see Table 4, without using any active (trim coils for field integrals and copper strips for the angular kicks) or passive (shimming for both field or phase errors) correction scheme. The SESAME EPU maps are shown in Appendix A.

The betatron beta beat is given by;

$$Beta - Beat[\%] = \frac{\beta_{bare} - \beta_{\mathrm{mod}}}{\beta_{bare}} \times 100\%$$

Where β_{bare} is the beta value for the bare lattice and β_{mod} is the beta value with the EPU magnet engaged at different modes of operation.

The vertical beta beat is not that significant, for the vertical mode of operation a maximum beta beat of 0.5 %, because of the low β_z value at the EPU location whereas the horizontal beta beat is rather significant, the worst case is with the vertical mode of operation where the peak horizontal field is B_x = 0.9724 T, mainly due to the high β_x value of 13.3m. The beta beats in both planes for all modes of operation are shown in Figures 34 and 35. The quadrupole doublet flanking the EPU magnet can be used to compensate for the beat beats in both planes and restore the tunes to the bare lattice values [1]. Table 5 shows the change in the strength of the quadrupole doublet to match the beta beats in both planes.

Table 5. Changes in strength of the quadrupole doublet to match the EPU's effect.

Mode of operation	Bare Latice		Matched lattice		Percentage [%]		Tunes
	QF	QD	QF	QD	QF	QD	Q_x / Q_z
Horizontal	2.03217	-1.22628	2.02069	-1.20057	-0.56	-2.09	7.2300 / 6.1900
Circular	2.03217	-1.22628	2.04797	-1.23976	+0.78	+1.10	7.2300 / 6.1900
Vertical	2.03217	-1.22628	2.06450	-1.26312	+1.59	+3.00	7.2300 / 6.1900

The map describing the EPU device has a finite size, ±30 mm in x-axis and ±5 mm in z-axis, which is considered as a physical limitation in the BETA code. Tracking the particles for 500 turns within this map (aperture) for the three modes of operation has not lead to significant reduction in the dynamic aperture of the SESAME lattice, see Figure 35.

In Appendix B, the feasibility of housing SESAME EPU in a long straight section of the SESAME lattice has been presented.

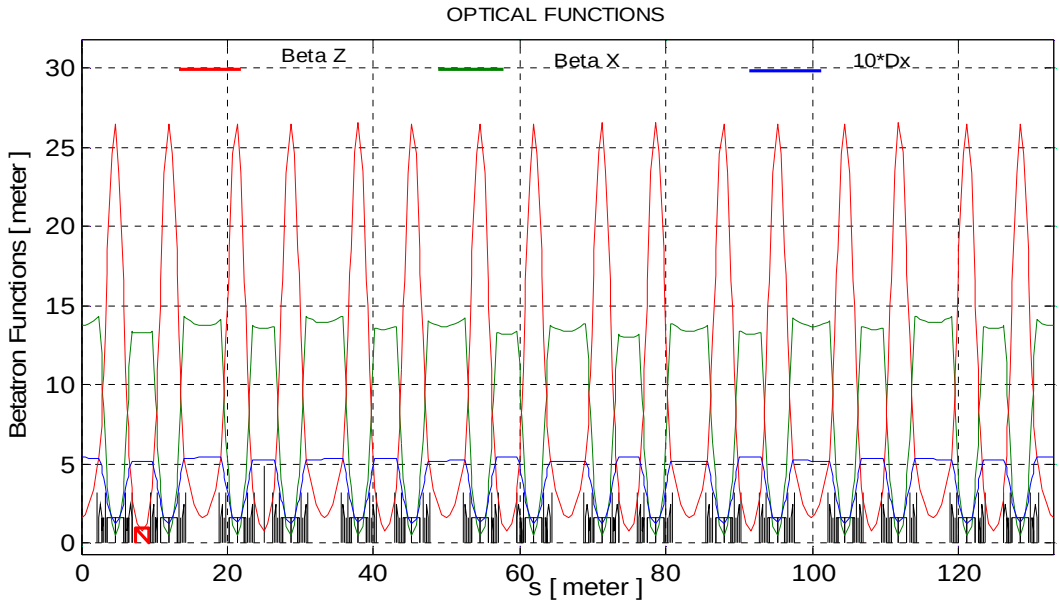

Figure 31. Machine functions for the horizontal undulator phase, The EPU magnet in red.

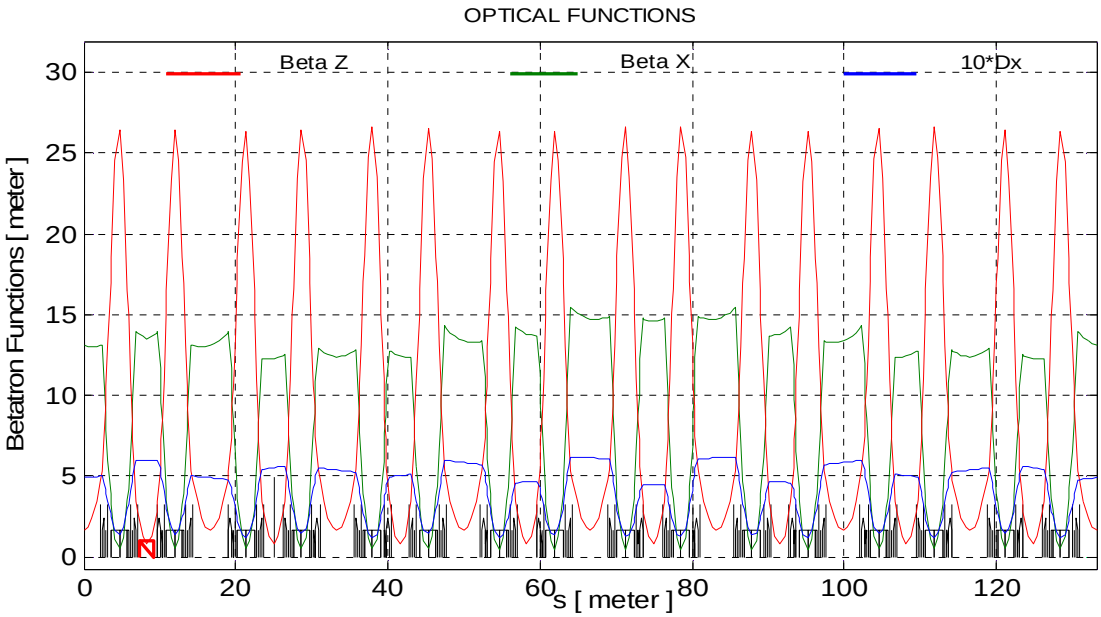

Figure 32. Machine functions for the vertical undulator phase, The EPU magnet in red.

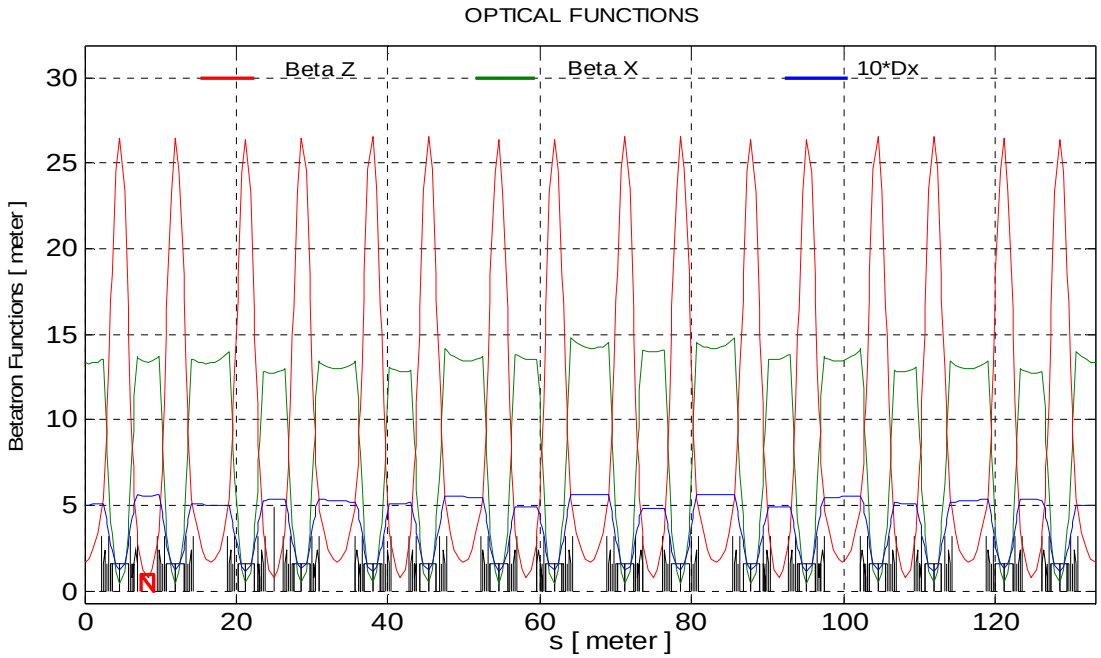

Figure 33. Machine functions for the circular undulator phase, The EPU magnet in red.

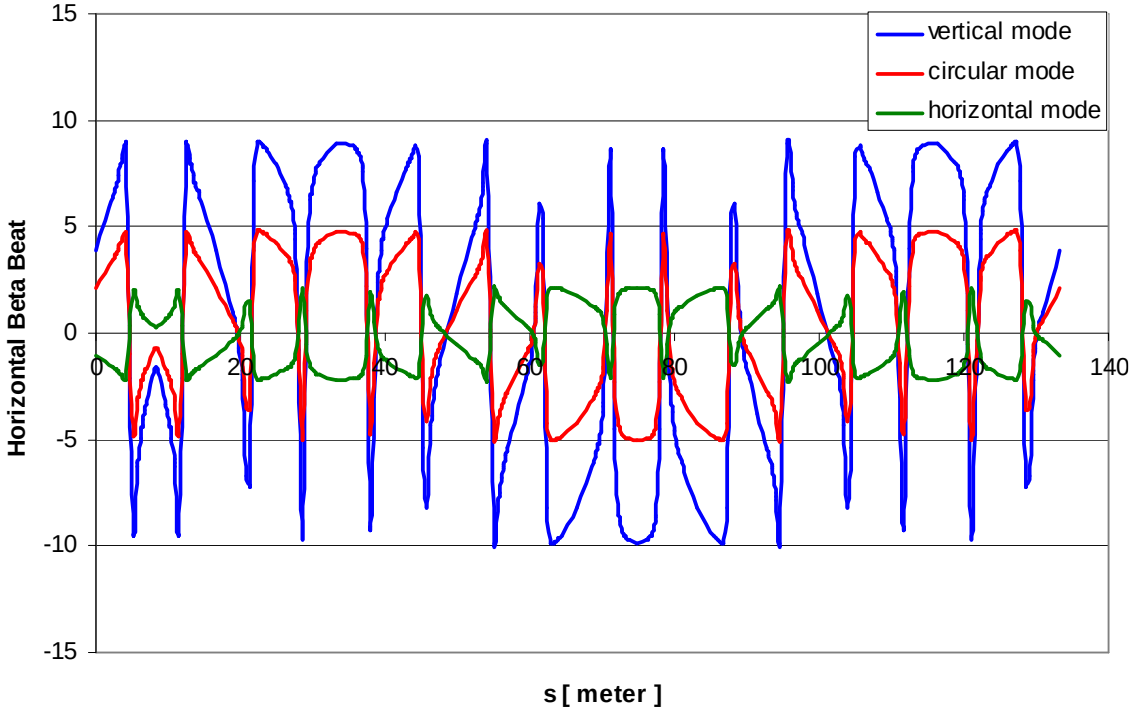

Figure 34. Horizontal beta beat for all undulator phases before matching.

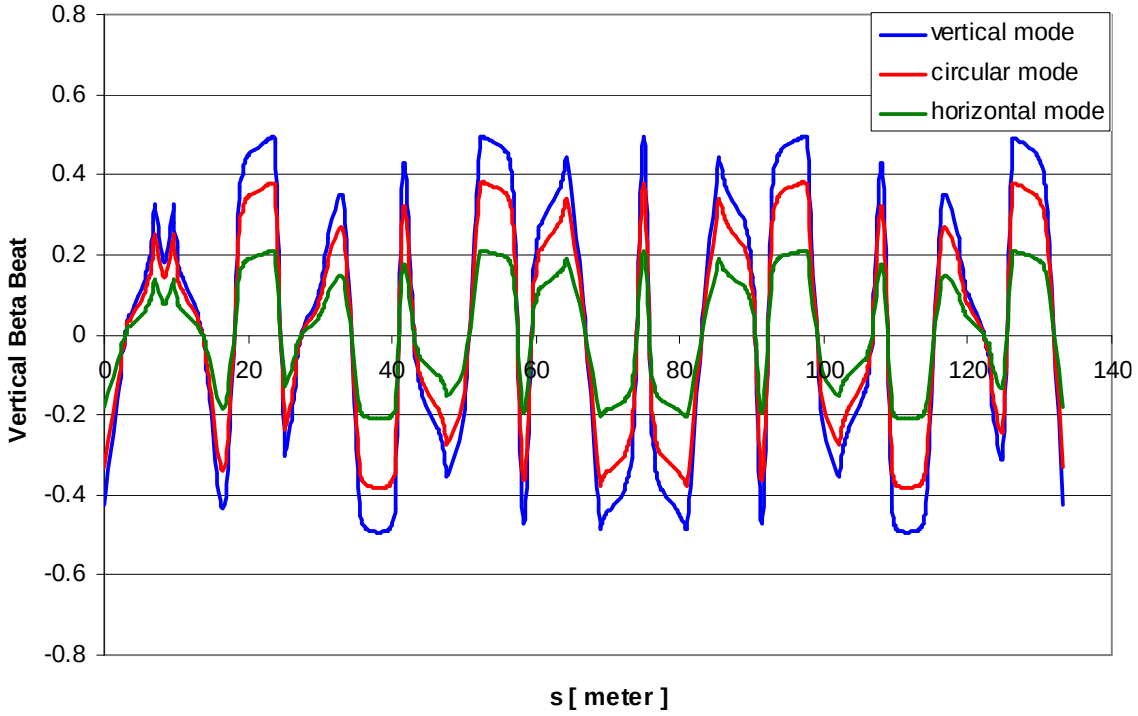

Figure 35. Vertical beta beat for all undulator phases before matching.

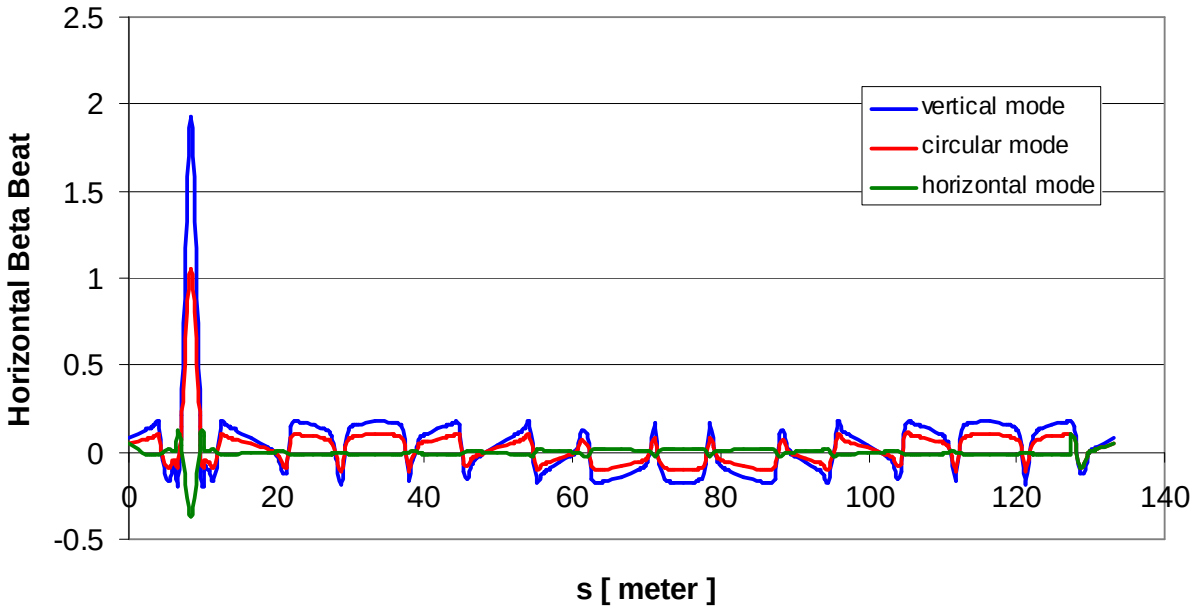

Figure 36. Horizontal beta beat for all undulator phases after matching.

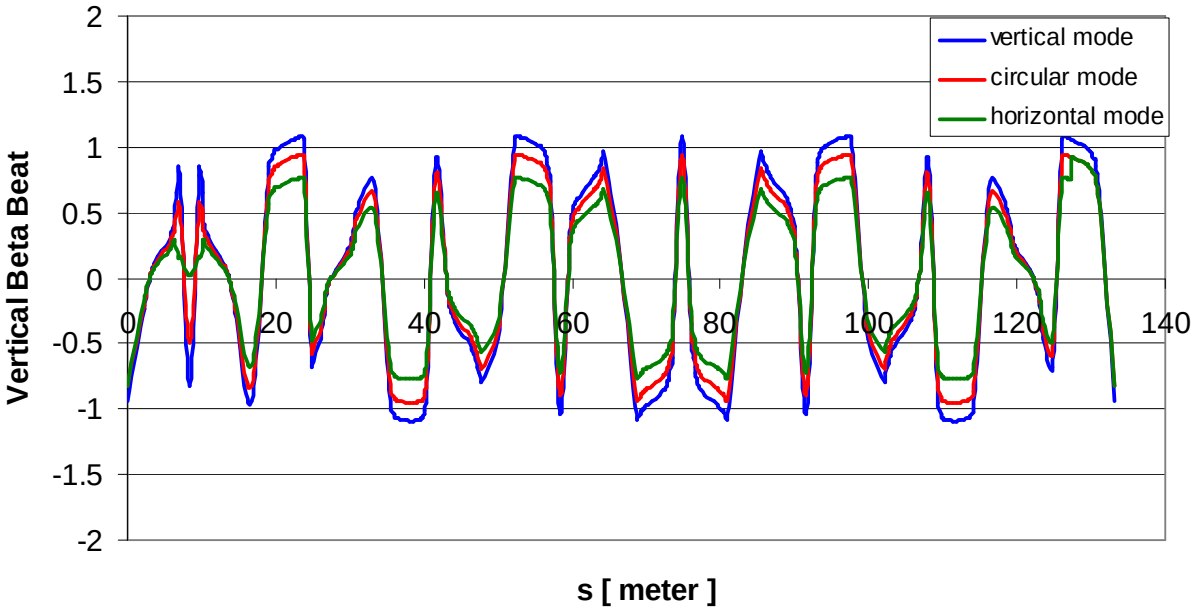

Figure 37. Vertical beta beat for all undulator phases after matching.

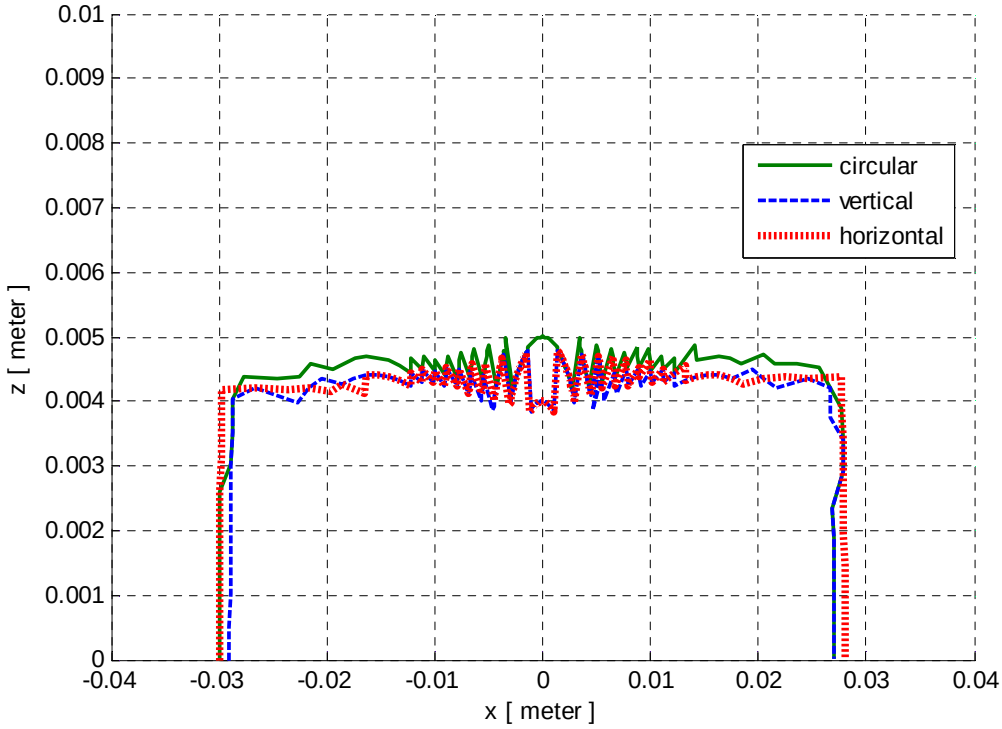

Figure 38. Dynamic aperture for the SESAME lattice with the mapped EPU magnet engaged.

5. MAGNETIC FORCE

There are three types of magnetic forces on the magnet assemblies, transverse, longitudinal and vertical forces which vary with the undulator gap and phase. The transverse force is due to the 1 mm space between the left and right sub-assemblies. Figures 39 to 41 show the three types of the magnetic forces on top right sub-assembly from the full-size undulator. In Figure 39, the transverse force is repulsive for small phase values, attractive for large values and not dependant on the undulator gap. In Figure 40, the longitudinal force is anti-parallel to the movement and has the opposite behavior to the other sub-assembly. In Figure 41, the vertical force is attractive for small phase values and repulsive for large values.

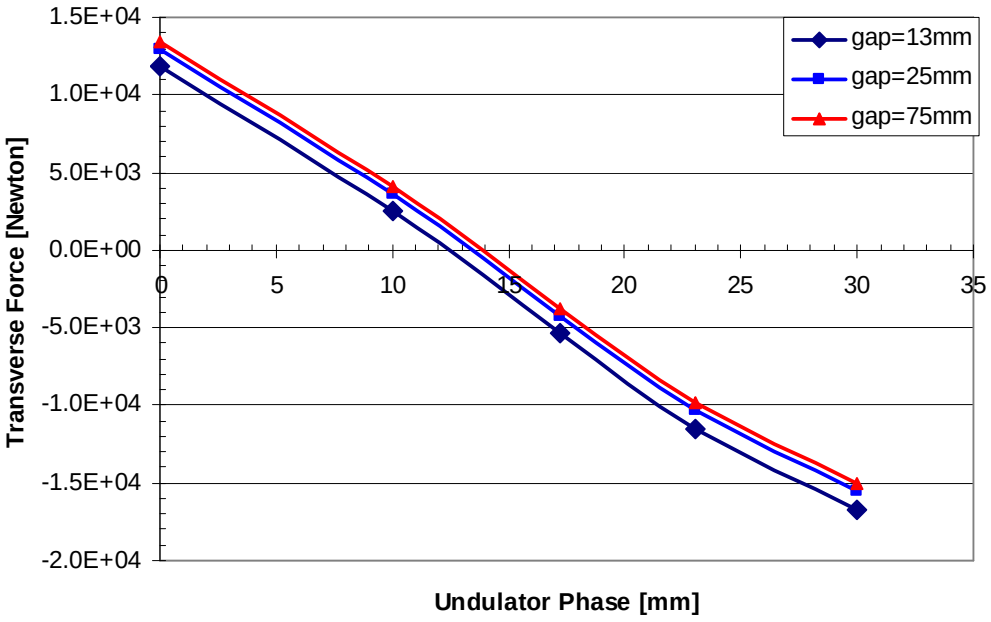

Figure 39. Transverse magnetic force on the top right sub-assembly.

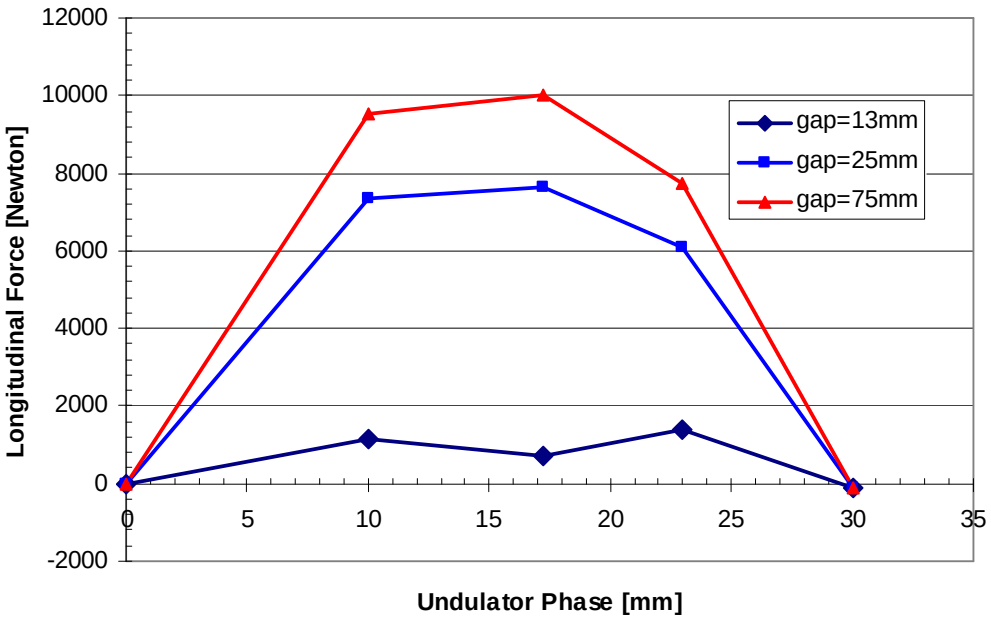

Figure 40. Longitudinal magnetic force on the top right sub-assembly.

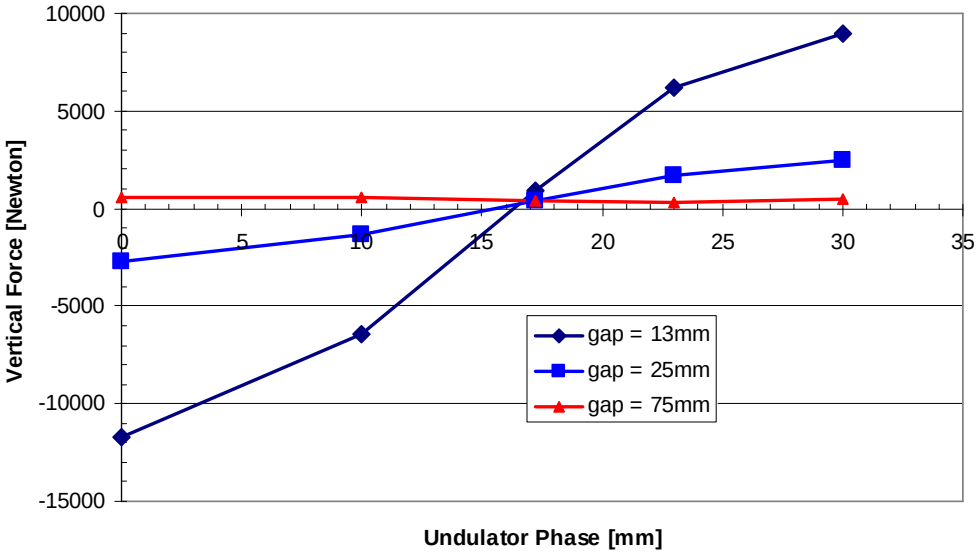

Figure 41. Vertical magnetic force on the top right sub-assembly.

6. PHOTON OUTPUT

The magnetic field model has been used to calculate the synchrotron radiation output from the SESAME EPU undulator using the SPECTRA code [12]. The broadening of the peaks due to emittance and energy spread are included in the calculations. The machine parameters used to evaluate the photon flux density and brilliance are found in Table 4.
Figures 42 to 47 show the photon flux density and brilliance for all mode of operation of the SESAME EPU undulator. The overlap between the first four harmonics is very good for the horizontal and the vertical modes of operation.

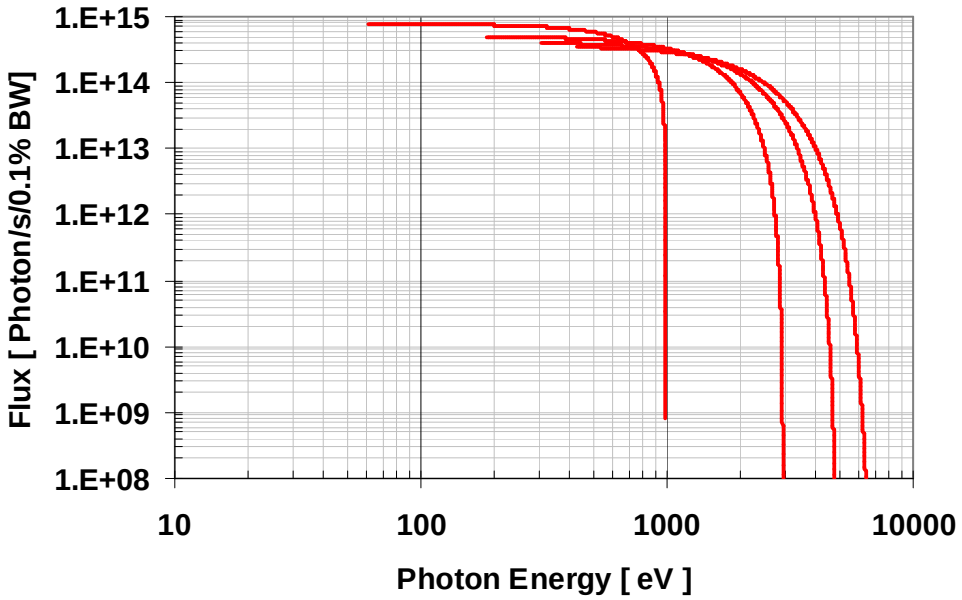

Figure 42. SESAME EPU photon flux density for the horizontal undulator phase.

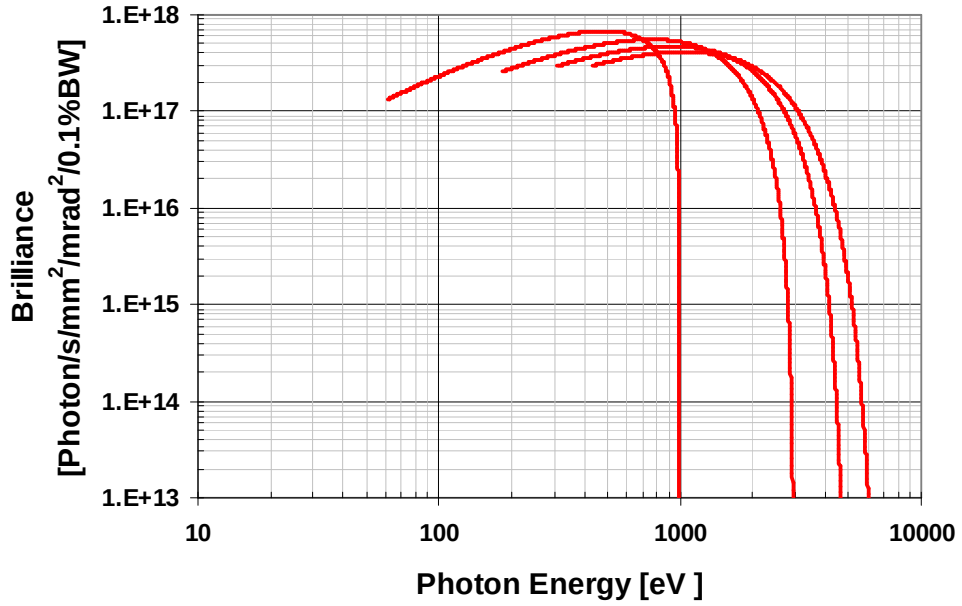

Figure 43. SESAME EPU estimated brilliance for the horizontal undulator phase.

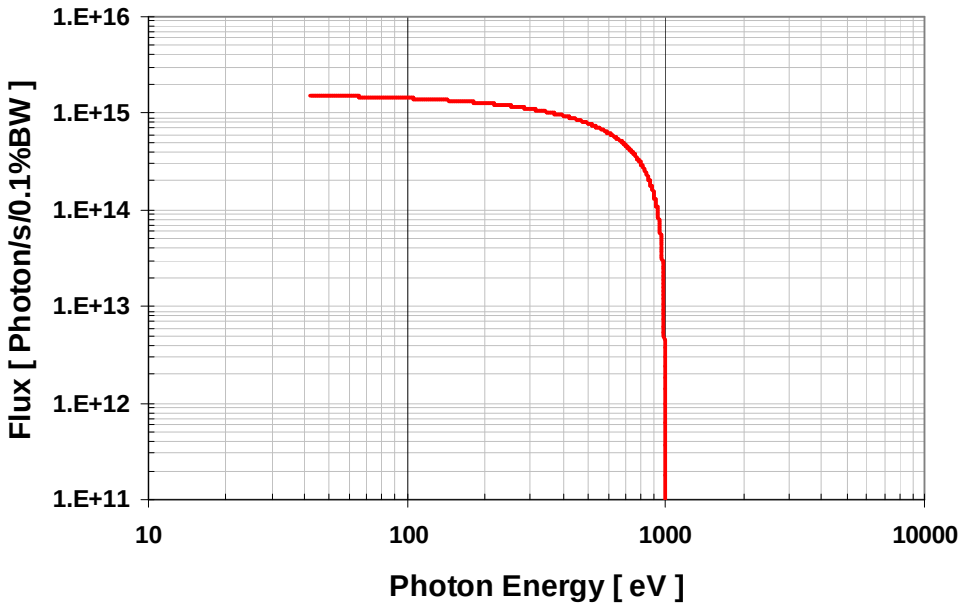

Figure 44. SESAME EPU photon flux density for the circular undulator phase.

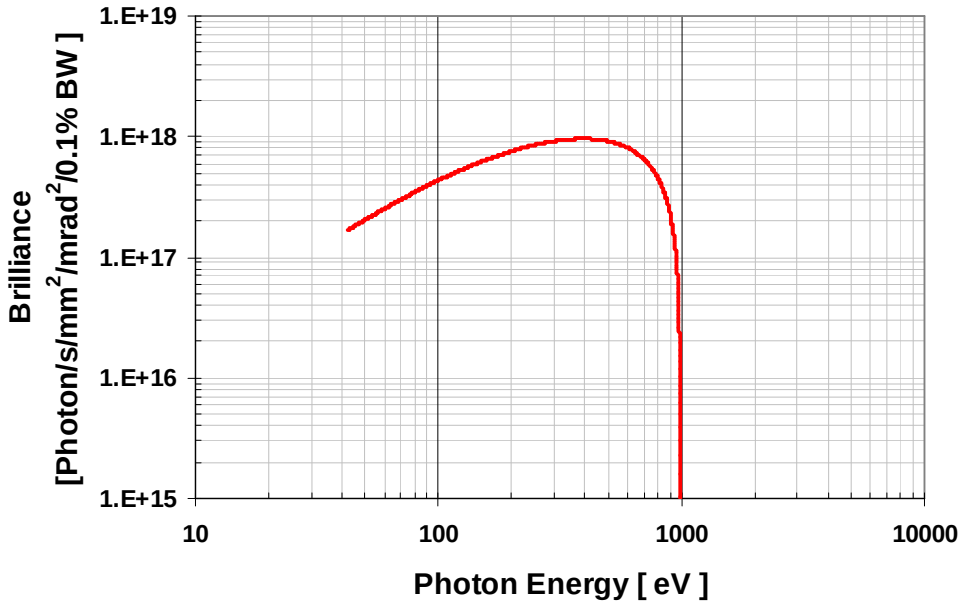

Figure 45. SESAME EPU estimated brilliance for the circular undulator phase.

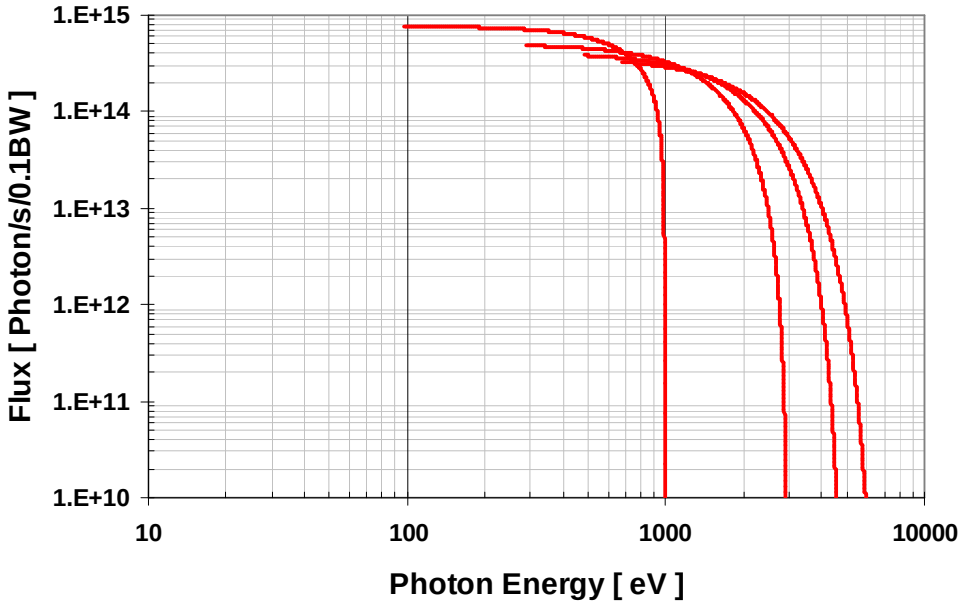

Figure 46. SESAME EPU photon flux density for the vertical undulator phase.

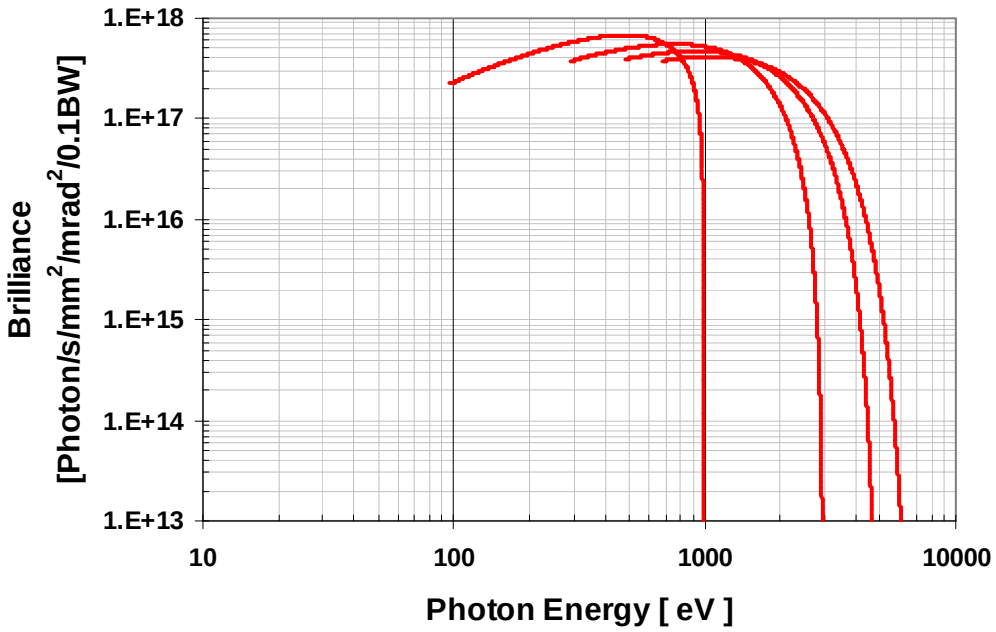

Figure 47. SESAME EPU estimated brilliance for the vertical undulator phase.

7. CONCLUSIONS AND FURTHER WORK

A variable polarization undulator of the Apple-II type has been designed for the SESAME light source. The device is designed to operate in the helical mode, i.e. horizontally, vertically and elliptically polarized light, which satisfies the demand of the SESAME users. This design provides low field integrals in both planes that can be corrected with trim coils and hence, maintain very low position and angle deviation of the electron beam through the undulator.

The dynamic aperture of the SESAME lattice has not suffered a severe reduction due to the inclusion of the EPU magnet and the effect on the emitance and energy spread is negligible. The quadrupole doublets flanking the EPU magnet are adequate to compensate for the beta beats in both planes.

A further work, which needs to be thoroughly investigated, is summarized below;

- Modeling of the trim coils to further reduce the field integrals.
- Modeling of a copper strips to further reduce the angular kick by generating a normal quadrupole field.
- Modeling of shims for phase and field errors.
- Investigation of the power loading on the vacuum chamber for all modes of operation.
- Using the estimated magnetic forces in order to check the effect of deflection of the magnet block holders and the magnet girder.

REFERENCES

[1] G. Vignola, M. Attal, " SESAME Lattice", Technical Note: O-1, December 21, 2004, Amman, Jordan

[2] 4th SESAME Users Meeting,6-8 Dec. 2005 Dead Sea, Jordan.

[3] Sasaki, "Analysis for a planar variably-polarizing undulator", Nuclear Instruments and Method in Physics Research A, NIMA 347, 1994.

[4] P. Elleaume, O. Chubar, J. Chavanne, "Computing 3D Magnetic Field for Insertion Devices", Proceedings of PAC'97, Vancouver.

[5] J. Chavanne, P. Elleaume, P. Van Vaerenbergh, "End Field Structures for Linear/Helical Insertion Devices", Proceedings of PAC'99, New York.

[6] R. P. Walker, 'Insertion devices, Undulators and Wigglers', CERN Accelerator School, CAS Proceedings, 98-04, pp. 129.

[7] P. Elleaume, "A New Approach to the Electron Beam Dynamics in Undulators and Wigglers", Proceedings of EPAC'92, Berlin.

[8] B. Diviacco, et. al. "Development of elliptical undulator for Elettra", Proceedings of EPAC'00, Vienna, Austria.

[9] K. I. Blomqvist, private communications.

[10] H. Wiedemann, "Particle accelerator physics" Vol. 1, Springer-Verlag, Berlin Heidelberg 1993.

[11] L. Farvacque, et. al. "BETA users' guide", Grenoble, France, 3rd edition, July 2001.

[12] http://radiant.harima.riken.go.jp/spectra/index.html

APPENDIX A
ANGULAR KICK MAPS FOR THE SESAME EPU

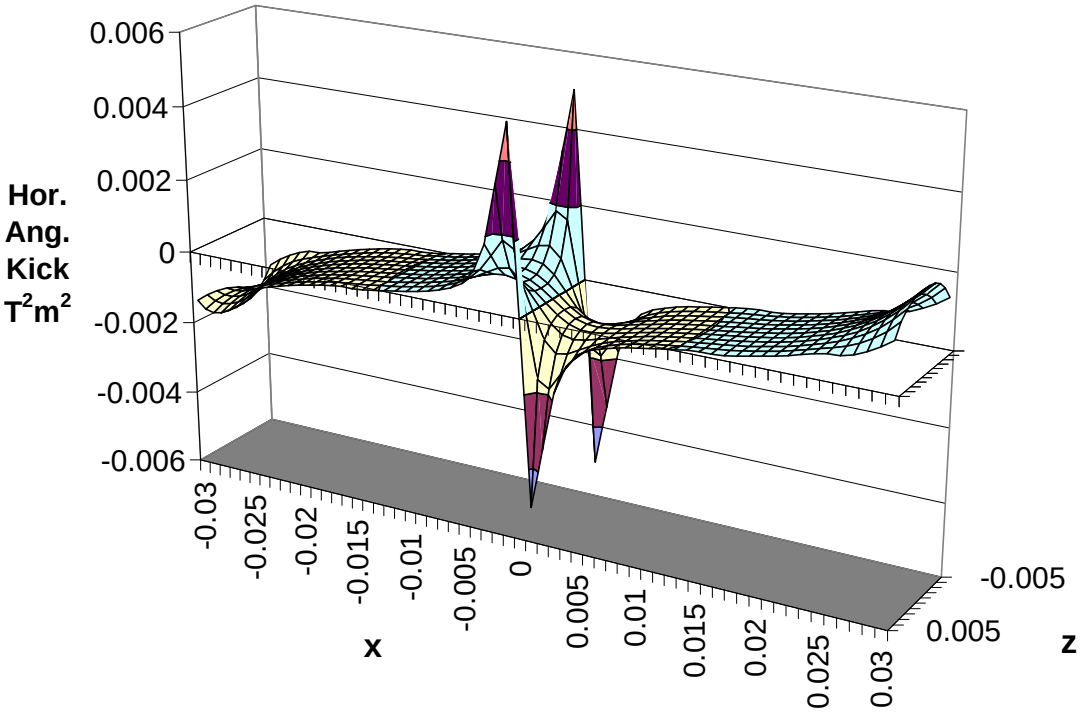

Figure A1.Horizontal angular kick map for the horizontal mode of operation.

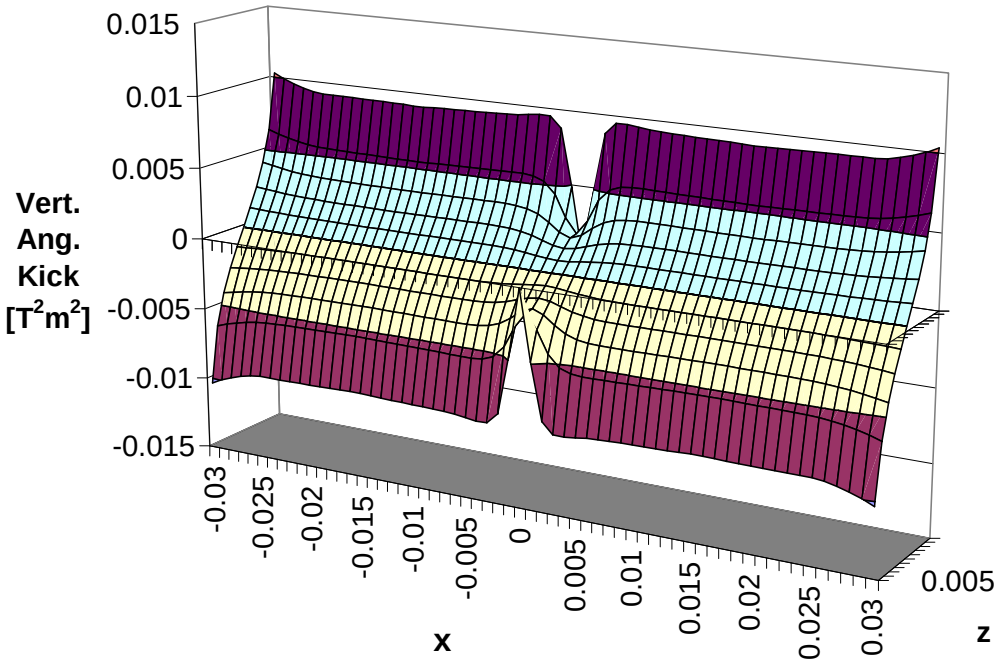

Figure A2.Vertical angular kick map for the horizontal mode of operation.

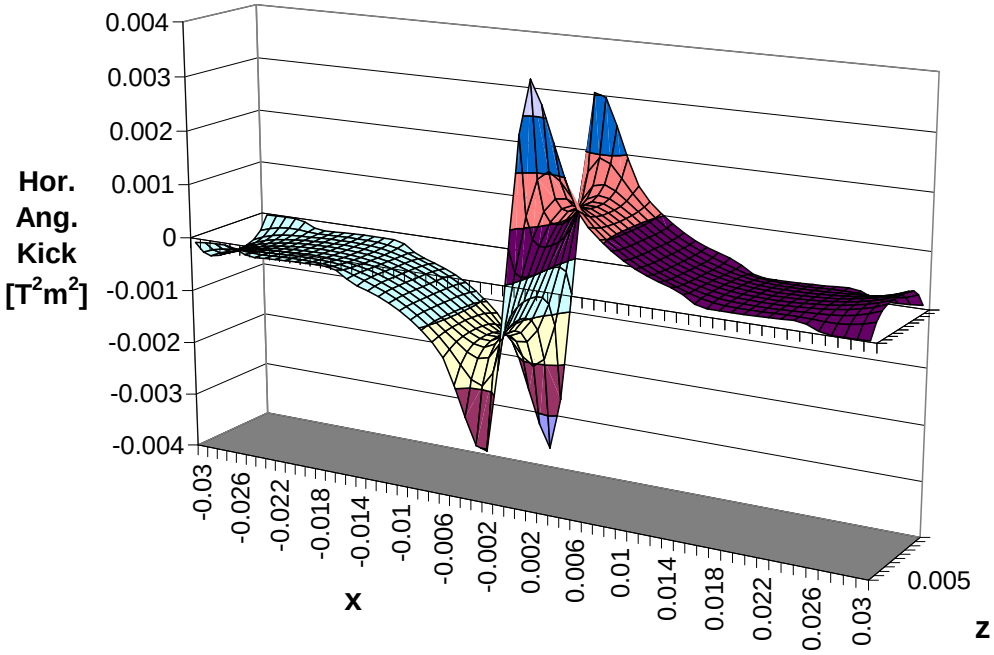

Figure A3. Horizontal angular kick map for the circular mode of operation

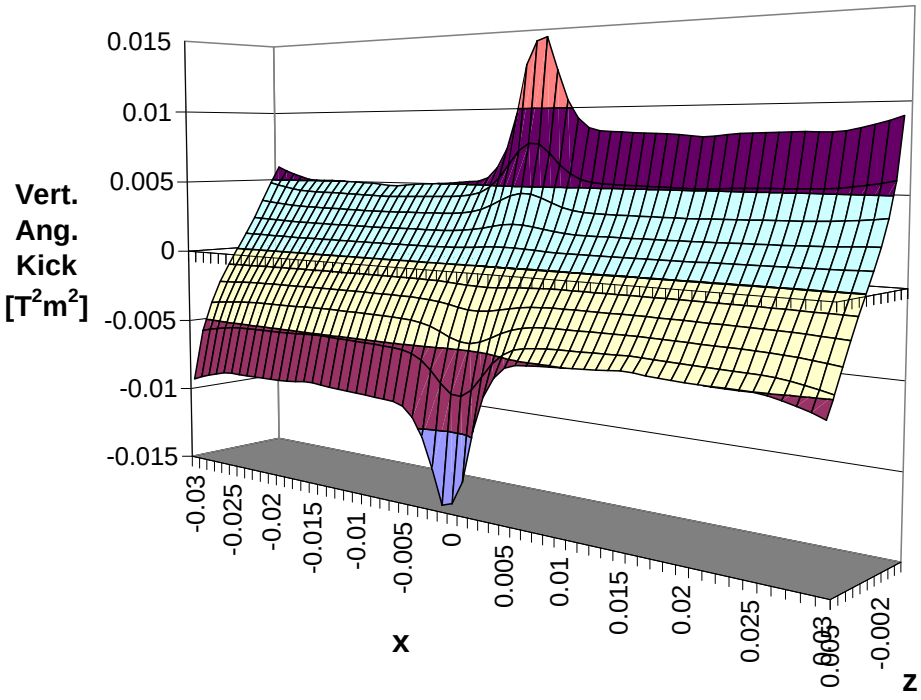

Figure A4. Vertical angular kick map for the circular mode of operation

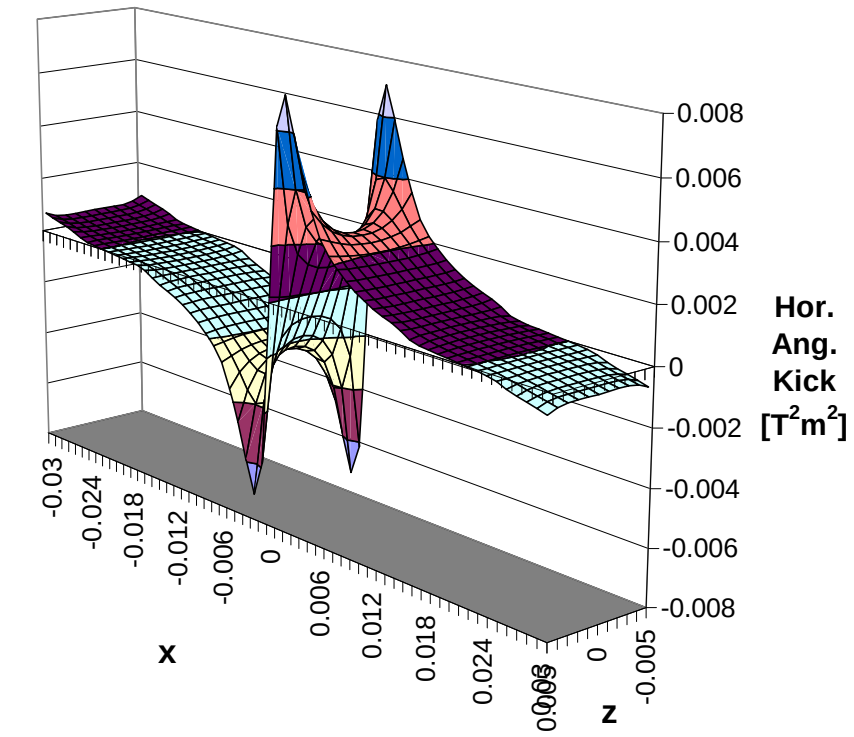

Figure A5. Horizontal angular kick map for the vertical mode of operation.

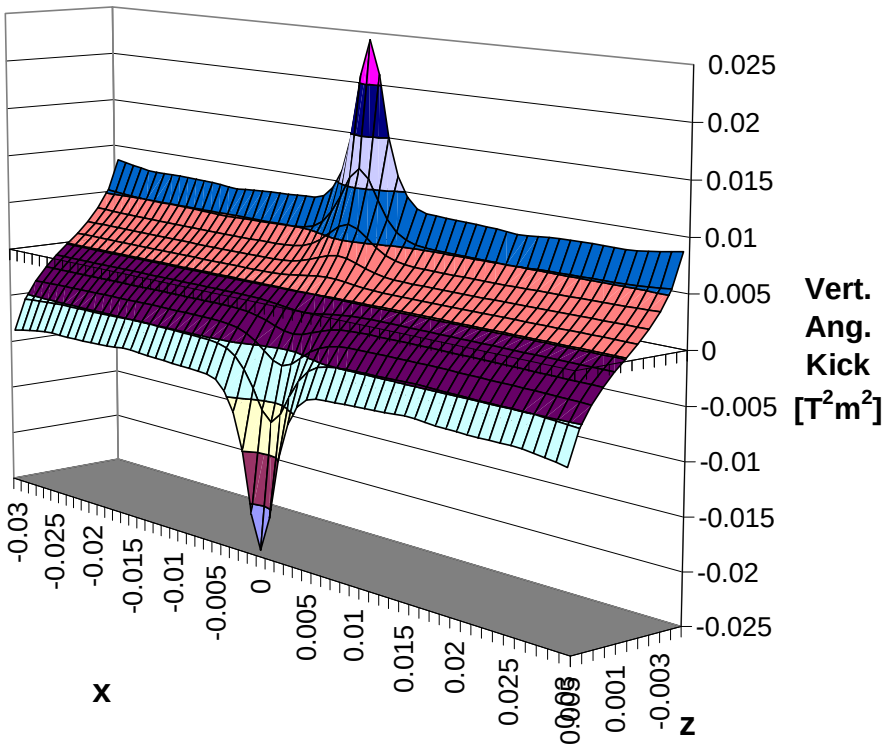

Figure A6. Vertical angular kick map for the vertical mode of operation

APPENDIX B
FEASIBILITY OF HOUSING SESAME EPU IN A LONG STRAIGHT SECTION

The feasibility of housing the SESAME EPU in a long straight section of the SESAME lattice has been investigated. The betatron functions in the middle of the long straight section are given Table B1;

Table B1. Betatron functions in the middle of long straight section

$\beta_x / \alpha_x / \eta_x / \eta'_x$	13.61 m / 0 / 0.53m / 0
$\beta_z / \alpha_z / \eta_z / \eta'_z$	1.65 m / 0 / 0 / 0

The machine functions are shown in Figures B1 to B3 for all modes of operation of the EPU magnet. The influence in the horizontal plane is comparable to the case of short straight section but more pronounced in the vertical plane due to larger β_z. This can be compensated by using the flanking quadrupole doublet and achieving a maximum beta beats of 3.1 % in the horizontal plane and 2.5 % in the vertical plane, See Figures B4 and B5. The change in the quadrupoles strength is shown Table B2;

Table B2. Changes in strength of the quadrupole doublet to match the EPU's effect.

Mode of operation	Bare Latice		Matched lattice		Percentage [%]		Tunes
	QF	QD	QF	QD	QF	QD	Q_x / Q_z
Horizontal	2.03217	-1.22628	2.01916	-1.19338	-0.64	-2.68	7.2300 / 6.1900
Circular	2.03217	-1.22628	2.04734	-1.23839	+0.75	+0.99	7.2300 / 6.1900
Vertical	2.03217	-1.22628	2.06452	-1.26516	+1.59	+3.17	7.2300 / 6.1900

The degradation in the dynamic aperture is more severe, i.e. a loss of approximately 20%, see Figure B6. Furthermore, the electron beam size is larger than the one in the short straight section resulting in lower brilliance.

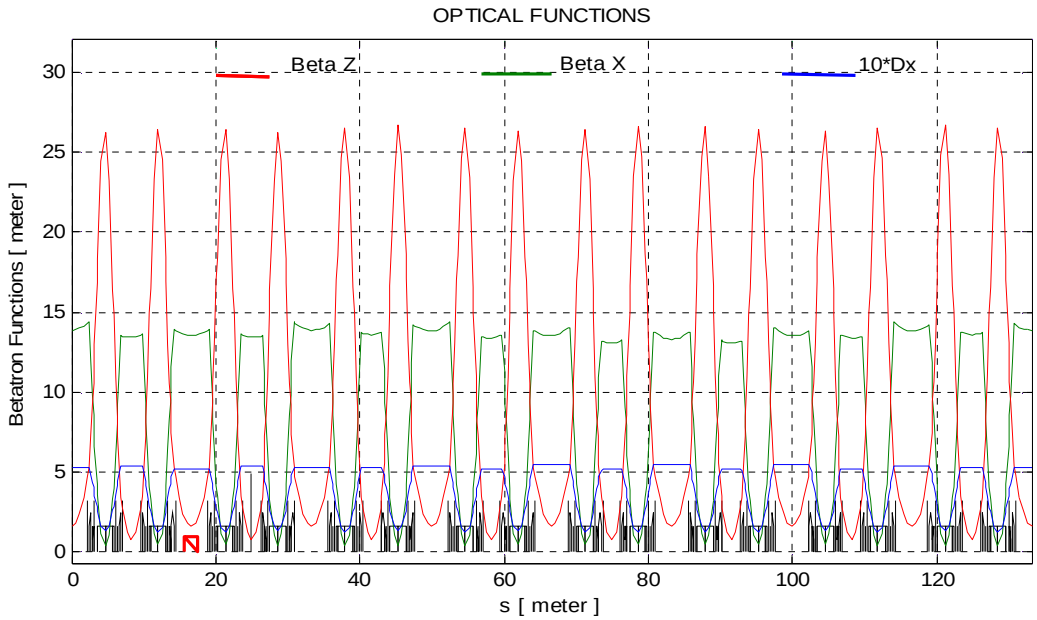

Figure B1. Machine functions for the horizontal undulator phase, The EPU magnet in red.

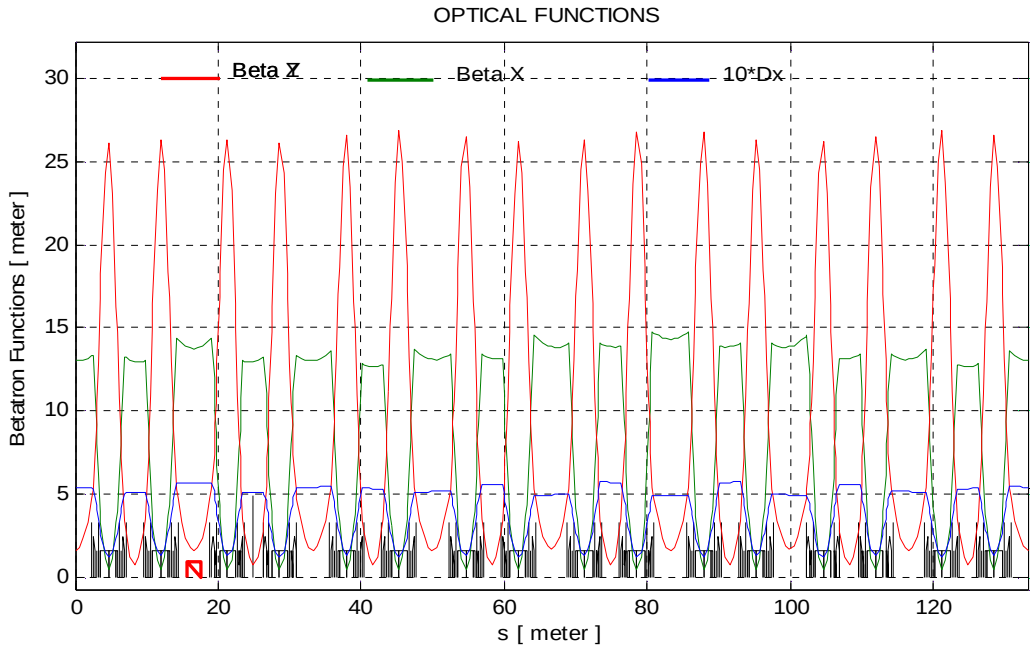

Figure B2. Machine functions for the circular undulator phase, The EPU magnet in red.

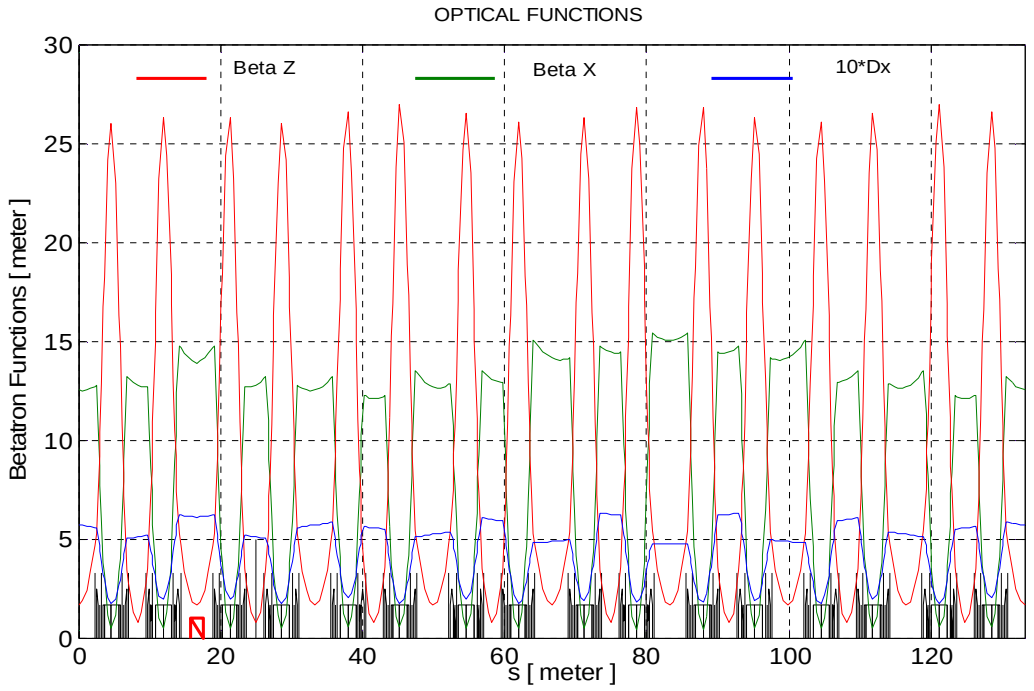

Figure B3. Machine functions for the vertical undulator phase, The EPU magnet in red.

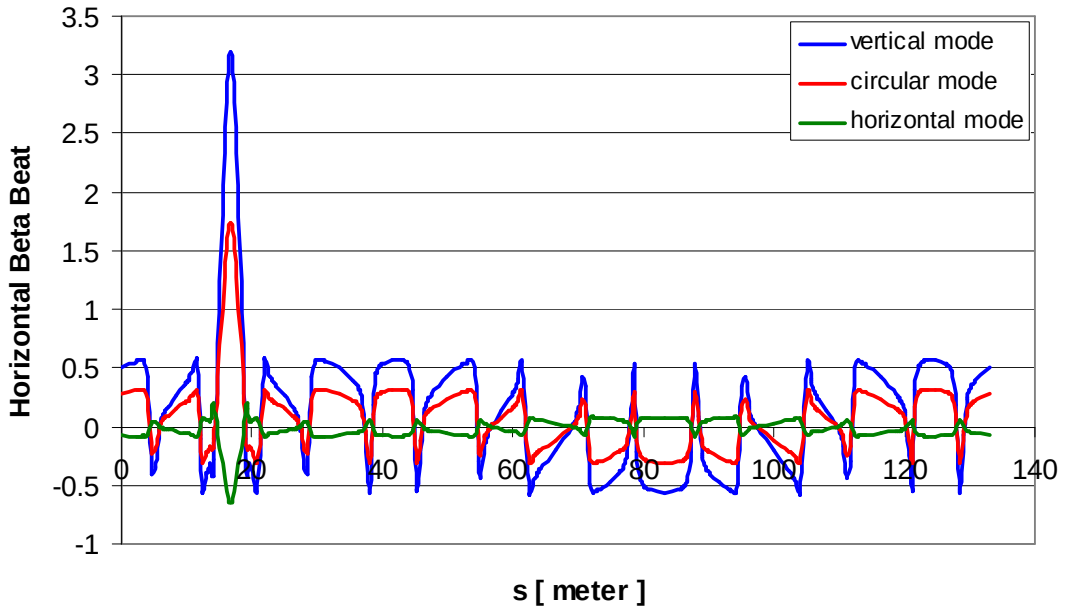

Figure B4. Horizontal beta beat for all undulator phases after matching.

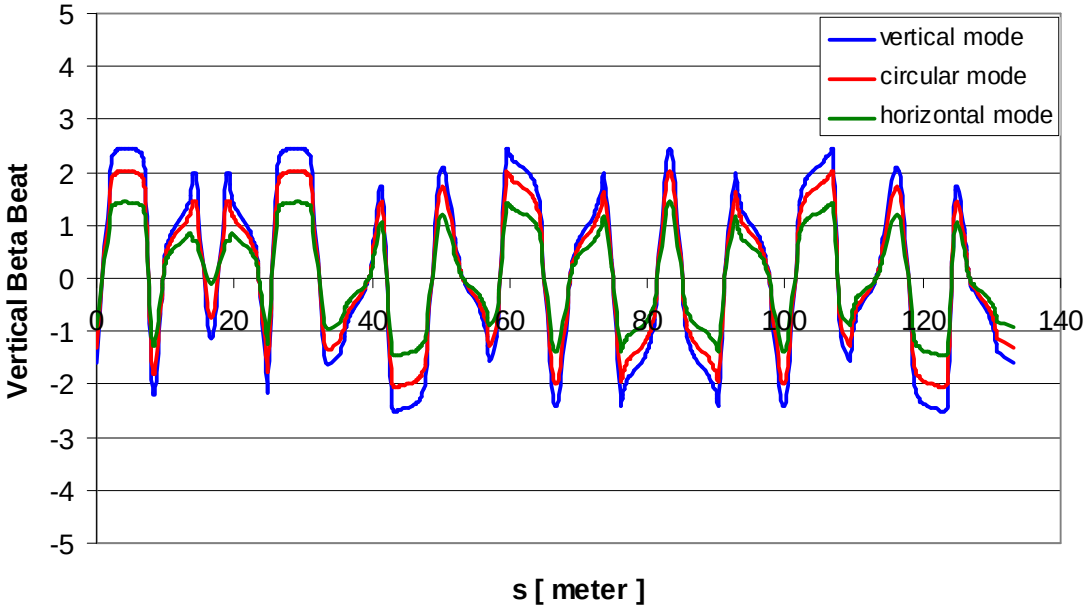

Figure B5. Vertical beta beat for all undulator phases after matching.

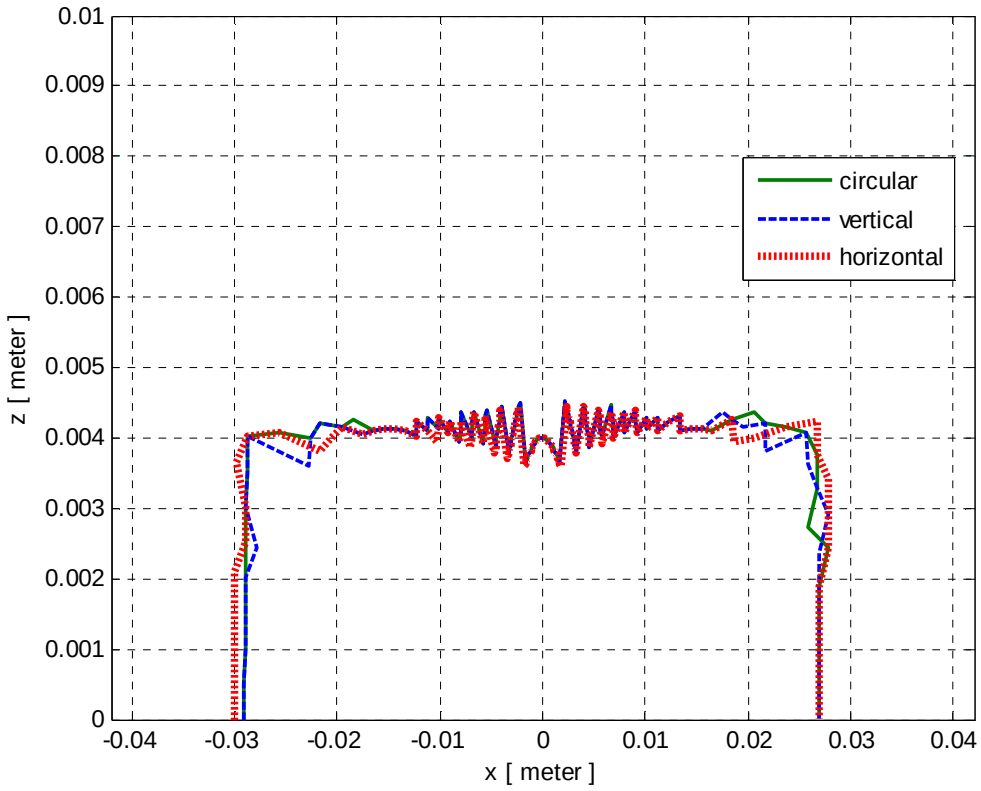

Figure B6. Dynamic aperture for the SESAME lattice with the mapped EPU magnet engaged in a long straight section.